bioRxiv preprint doi: https://doi.org/10.1101/2022.05.13.491370; this version posted May 13, 2022. The copyright holder for this preprint (which was not certified by peer review) is the author/funder, who has granted bioRxiv a license to display the preprint in perpetuity. It is made available under aCC-BY-NC 4.0 International license.

Vitamin K-dependent carboxylation of junctate regulates calcium flux and adaptation to metabolic stress in β-cells

Julie Lacombe[1,7,*], Kevin Guo[1,2,7], Jessica Bonneau[1,3], Denis Faubert[4], Florian Gioanni[1], Alexis Vivoli[5], Sarah M. Muir[1], Soraya Hezzaz[1], Vincent Poitout[3,6], Mathieu Ferron[1,2,3,6, *]

[1] Molecular Physiology Research Unit, Institut de Recherches Cliniques de Montréal, Montréal, Québec, Canada, H2W 1R7.
[2] Division of Experimental Medicine, McGill University, Montréal, Québec, Canada.
[3] Programme de Biologie Moléculaire, Université de Montréal, Montréal, Québec, Canada.
[4] Mass spectrometry and Proteomics Platform, Institut de Recherches Cliniques de Montréal, Montréal, Québec, Canada, H2W 1R7.
[5] Montreal Diabetes Research Center, Centre de Recherche du Centre Hospitalier de l'Université de Montréal (CRCHUM), Montréal, Québec, Canada, H2X 0C1.
[6] Département de Médecine, Université de Montréal, Montréal, Québec, Canada.
[7] Co-first authors.

* Correspondence to:

Mathieu Ferron, PhD
Institut de Recherches Cliniques de Montréal
110 Ave. des Pins O.
Montréal, QC,
H2W 1R7, Canada
Phone: 514-987-5754
Fax: 514-987-5649
Email: mathieu.ferron@ircm.qc.ca

Julie Lacombe, PhD
Institut de Recherches Cliniques de Montréal
110 Ave. des Pins O.
Montréal, QC,
H2W 1R7, Canada
Phone: 514-987-5780
Email: julie.lacombe@ircm.qc.ca

bioRxiv preprint doi: https://doi.org/10.1101/2022.05.13.491370; this version posted May 13, 2022. The copyright holder for this preprint (which was not certified by peer review) is the author/funder, who has granted bioRxiv a license to display the preprint in perpetuity. It is made available under aCC-BY-NC 4.0 International license.

SUMMARY

Vitamin K (VK) is a micronutrient necessary for the γ-carboxylation of glutamic acids. This post-translational modification occurs in the endoplasmic reticulum (ER) and affects secreted proteins. Clinical studies have recently implicated VK in the pathophysiology of diabetes, but the underlying molecular mechanism remains unknown. Here, we show that β-cells lacking γ-carboxylation fail to adapt their insulin secretion in response to glucose in the context of age-related insulin resistance or diet-induced β-cell stress. Conversely, VK supplementation protects β-cells from ER stress-induced apoptosis. We identified junctate as a γ-carboxylated ER-resident protein expressed in β-cells, whose carboxylation is dysregulated in diabetic mouse models. Mechanistically, γ-carboxylation of junctate maintains basal cytosolic calcium levels and restrains store-operated calcium entry, by diminishing STIM1 and Orai1 puncta formation at the plasma membrane. These results reveal a critical role for γ-carboxylation in the regulation of calcium flux in β-cells and in their capacity to adapt to metabolic stress.

KEYWORDS

γ-carboxylation; ER stress; store-operated calcium entry; Vitamin K; GGCX; Junctate; β-cells; insulin secretion; diabetes

bioRxiv preprint doi: https://doi.org/10.1101/2022.05.13.491370; this version posted May 13, 2022. The copyright holder for this preprint (which was not certified by peer review) is the author/funder, who has granted bioRxiv a license to display the preprint in perpetuity. It is made available under aCC-BY-NC 4.0 International license.

INTRODUCTION

Type 2 diabetes (T2D) is a metabolic disorder characterized by insulin resistance, hyperglycemia and hyperinsulinemia (Hudish et al., 2019). Traditionally, T2D has been viewed as a diseased initiated by peripheral insulin resistance ultimately resulting in pancreatic β-cell dysfunction. However, recent studies suggest that uncontrolled and excessive insulin secretion by β-cells could be the driving force that elicits peripheral insulin resistance and metabolic complications in T2D (Mehran et al., 2012; Mittendorfer et al., 2022). Human and animal studies indicate that several factors can influence T2D susceptibility including age, genetic variants, and diet. Interestingly, many of these factors are thought to directly impact β-cell function (Solis-Herrera et al., 2000). Increased consumption of highly processed, calorie-rich, but nutrient-poor food is one possible contributor to the current T2D pandemic (Srour et al., 2020). Paradoxically, in Western countries, excess calorie intake is frequently associated with deficiency in a number of micronutrients, including trace elements such as zinc (Chabosseau and Rutter, 2016), and several vitamins (Kaidar-Person et al., 2008). Other studies have linked micronutrient deficiencies to an increased risk of diabetes (Hoffman et al., 2021; Via, 2012). Yet, the implication of micronutrients in β-cell function remains poorly understood.

Vitamin K (VK), a fat-soluble vitamin, functions as a co-factor during the γ-carboxylation reaction that converts glutamic acid (Glu) residues to γ-carboxyglutamic acid (Gla) residues in proteins transiting through the endoplasmic reticulum (ER). Two ER-resident enzymes are involved in this reaction, which together form the VK cycle: γ-glutamyl carboxylase (GGCX), and vitamin K oxidoreductase (VKORC1) (Lacombe and Ferron, 2018). GGCX requires reduced VK (VKH_2) as an essential cofactor, which upon carboxylation, is oxidized to VK epoxide (VKO) and then reconverted to VKH_2 by VKORC1. The presence of this post-translational modification in proteins results in higher affinity for calcium ions. Altogether, in vertebrates, less then 15 γ-carboxylated proteins have been identified so far, all of them being secreted proteins. Gamma-carboxylation is essential in the liver for the activity of several coagulation factors (e.g., prothrombin, factor IX, etc.), and in arteries and cartilage to modulate the activity of Matrix Gla Protein (MGP) which prevents extra-osseous tissue mineralization (Furie et al., 1999; Murshed et al., 2004). Gamma-carboxylation also negatively regulates the function of osteocalcin, a bone-derived hormone with pleiotropic actions (Ferron et al., 2015; Lee et al., 2007). Whether γ-carboxylation occurs on ER-resident proteins and regulates cellular functions in a cell-autonomous manner is currently unknown.

bioRxiv preprint doi: https://doi.org/10.1101/2022.05.13.491370; this version posted May 13, 2022. The copyright holder for this preprint (which was not certified by peer review) is the author/funder, who has granted bioRxiv a license to display the preprint in perpetuity. It is made available under aCC-BY-NC 4.0 International license.

Clinical and genetic data suggest that VK insufficiency or reduced VK intake are associated with an increased risk of developing metabolic syndrome or T2D (Beulens et al., 2010; Ibarrola-Jurado et al., 2012; Pan and Jackson, 2009; Zwakenberg et al., 2019). Two longitudinal studies found a positive association between low VK dietary intake and the risk of developing T2D (Beulens et al., 2010; Ibarrola-Jurado et al., 2012). It was also observed that 40% of morbidly obese patients are characterized by VK insufficiency and that low serum VK correlates positively with the presence of T2D in these subjects (Dihingia et al., 2018; Ewang-Emukowhate et al., 2015; Zwakenberg et al., 2019). Finally, VK supplementation in patients with T2D significantly decreased their fasting glucose and HbA1c blood concentrations (Karamzad et al., 2020; Rahimi Sakak et al., 2021). These clinical studies suggest a link between VK insufficiency and the risk of developing diabetes. However, they also raise important questions regarding the mechanism by which VK protects from T2D. Does VK directly affect β-cell function? If so, what are the cellular and molecular mechanisms involved, and which γ-carboxylated protein mediate the protective effect of VK?

In the current study, we aimed at answering these questions using a combination of unique genetic, cellular, and biochemical tools we developed to study γ-carboxylation. We show that GGCX and VKORC1, the two enzymes of the VK cycle, are expressed and active in mouse and human pancreatic islets and β-cells. Using loss-of-function models, we found that the inactivation of *Ggcx* impairs β-cell function in young mice exposed to a short bout of high-fat diet (HFD), and compromises β-cell survival in older animals fed a regular diet. Finally, we identify junctate as a novel γ-carboxylated ER-resident calcium-binding protein whose γ-carboxylation regulates basal cytosolic calcium levels and store-operated calcium entry (SOCE) in β-cells. These data demonstrate that γ-carboxylation plays a critical role in the capacity of β-cells to adapt to physiological stress, which is also supported by our observations that this enzymatic pathway is hyperactivated in diabetic mouse β-cells characterized by ER stress.

bioRxiv preprint doi: https://doi.org/10.1101/2022.05.13.491370; this version posted May 13, 2022. The copyright holder for this preprint (which was not certified by peer review) is the author/funder, who has granted bioRxiv a license to display the preprint in perpetuity. It is made available under aCC-BY-NC 4.0 International license.

RESULTS

Vitamin K-dependent carboxylation occurs in islets and β-cells

To identify tissue(s) involved in the beneficial effect of VK on glucose metabolism and T2D, we first examined GGCX and VKORC1 protein levels in different human tissues using the ProteomicsDB resource (Schmidt et al., 2018). This analysis revealed that pancreatic islets were ranked fourth and first for GGCX and VKORC1 protein expression respectively (Fig. 1A), in agreement with our own data showing that *Ggcx* and *Vkorc1* genes are highly expressed in mouse islets (Fig. S1A-B). To more precisely dissect *Ggcx* and *Vkorc1* expression within mouse islets, we used fluorescence-activated cell sorting (FACS) to isolate β-cells based on the expression of the fluorescent reporter protein tdTomato (Tom) conditionally expressed in the insulin-positive cells of $Ins1^{Cre/+}$;$Rosa26^{CAG\text{-}lox\text{-}stop\text{-}lox\text{-}tdTomato}$ mice. Using this strategy, we could obtain a pure β-cell population (Tom+), as demonstrated by the expression of the insulin genes *Ins1* and *Ins2*, and the absence of the other endocrine cell type markers *Gcg*, *Ppy* and *Sst*, which were highly expressed in the Tom- population (Fig. 1B). Further quantitative PCR (qPCR) analyses revealed that *Ggcx* and *Vkorc1* are expressed in β-cells and other islet endocrine cells (Fig. 1C). Single cell transcriptomics data (Consortium, 2018) confirmed *Ggcx* and *Vkorc1* endocrine pancreas expression whereas very few pancreatic exocrine cells express these genes (Fig. S1C-D). These results agree with another set of publicly available mouse islet transcriptomic data (DiGruccio et al., 2016). In addition, we found that GGCX and VKORC1 proteins are expressed at similar and higher levels respectively in purified β-cells as compared to whole islets (Fig. 1D). Previous studies have established that GGCX carboxylates itself in a VK-dependent manner in vitro and in vivo in liver (Berkner and Pudota, 1998; Lacombe et al., 2018). Using γ-carboxylated GGCX (Gla-GGCX) as a readout of a functional VK cycle, we demonstrated that carboxylation does take place in pancreatic islets and specifically in β-cells (Fig.1D). GGCX expression was also detected in the rat insulinoma cell line INS-1 832/3 and its γ-carboxylation induced following treatment with phylloquinone (vitamin K_1; VK_1), which is absent from cell culture media and fetal bovine serum (Haque et al., 2014) (Fig.1E). To determine the extent of γ-carboxylation in vivo in islets and β-cells, we isolated islets from $Ggcx^{ff}$; *Pdx1-Cre* and $Ggcx^{ff}$; *Ins1-Cre* mice in which *Ggcx* has been inactivated specifically in the pancreas or in β-cells respectively (Fig. 1F and Fig. S1E-F). Western blot analyses with a previously characterized α-Gla specific antibodies (Lacombe et al., 2018) revealed the presence of carboxylated proteins in islets and β-cells as demonstrated by the reduced α-Gla immunoreactivity in $Ggcx^{ff}$; *Pdx1-Cre* and $Ggcx^{ff}$; *Ins1-Cre* islets (Fig.1F). Finally, GGCX is also expressed in human islets and culturing them with VK_1 increased protein γ-carboxylation. Conversely, warfarin, an

bioRxiv preprint doi: https://doi.org/10.1101/2022.05.13.491370; this version posted May 13, 2022. The copyright holder for this preprint (which was not certified by peer review) is the author/funder, who has granted bioRxiv a license to display the preprint in perpetuity. It is made available under aCC-BY-NC 4.0 International license.

inhibitor of VK oxidoreductase activity (Shen et al., 2017), reduced it (Fig. 1G, Table S1). In agreement with previous studies (Berkner and Pudota, 1998; Lacombe et al., 2018), we also observed that GGCX migrates faster in the presence of warfarin because of its incomplete γ-carboxylation. Together, these data support the conclusion that VKORC1, GGCX and γ-carboxylated proteins are present in islets and β-cells.

Loss of γ-carboxylation induces a diabetic signature in islets

As a first step to determine the role of VK-dependent carboxylation in islets and β-cells, we analyzed the expression profile of *Ggcx*^{ff}*; Pdx1-Cre* islets by RNA-sequencing (RNAseq). In comparison to control *Ggcx*^{ff} islets, we found that 319 genes were differentially expressed in *Ggcx*^{ff}*; Pdx1-Cre* islets (adjusted *P* value ≤ 0.05; Table S2). We divided this set of genes into two groups based on whether their expression was increased (114 genes) or decreased (205 genes) following *Ggcx* inactivation in islets, then completed a series of bioinformatics analyses on each group. Gene set enrichment analyses with Gene Ontology revealed that many biological processes implicated in the response to ER stress were significantly enriched within the group of genes repressed by *Ggcx* loss of function, such as *ER-nucleus signaling pathway*, *positive regulation of response to ER stress*, *regulation of response to ER stress*, *I-kappaB kinase/NF-kappaB signaling* and *regulation of apoptotic signaling pathway* (Fig.2A). Similarly, when we interrogated the KEGG pathway database, we found that this group of genes was enriched for pathways such as *apoptosis*, *protein processing in ER* and *NF-kappa B signaling pathway* (Fig.2B). Using the UniProt annotated keywords database, we found, in the group of genes that were upregulated in *Ggcx*^{ff}*; Pdx1-Cre* islets, a very strong enrichment for protein keywords related to the secretory pathway (e.g., *glycoprotein, signal, secreted, disulfide bond* and *extracellular matrix*; Fig. 2C). Based on these observations, we hypothesized that the capacity of islet cells to respond and adapt to ER stress might be deficient in the absence of γ-carboxylation, potentially leading to impaired β-cell function. In support of this notion, we found that a network of genes previously implicated in the β-cell response to ER stress, including *Ddit3* (CHOP), *Atf4*, *Eif2ak3* (PERK), *Herpud1*, *Trib3*, *Pdia4*, *Ppp1r1a* and *Atp2a2* (SERCA2) (Johnson et al., 2014; Sharma et al., 2021), was down-regulated in absence of γ-carboxylation (Fig. 1D).

We next determined to which extent the transcriptome of *Ggcx*^{ff}*; Pdx1-Cre* islets intersected with the gene expression profile of islets from pre-diabetic (adult C57BL/6 mice on HFD for 8 weeks) or diabetic (8-weeks old *Lepr*$^{db/db}$ and 7-weeks old *Ire1α*^{ff}*; Ins2-Cre*$^{ERT/+}$) mouse models (Lee et al., 2020;

bioRxiv preprint doi: https://doi.org/10.1101/2022.05.13.491370; this version posted May 13, 2022. The copyright holder for this preprint (which was not certified by peer review) is the author/funder, who has granted bioRxiv a license to display the preprint in perpetuity. It is made available under aCC-BY-NC 4.0 International license.

Motterle et al., 2017; Wang et al., 2012). We found that 75% of the up- and 45% of the down-regulated genes in *Ggcx*^{ff}*; Pdx1-Cre* islets were similarly dysregulated in at least one of these mouse models (Fig. 2E). About one-third of these genes are coding for proteins found within the secretory pathway (Fig.2F). The fold enrichment of the genes comparably regulated between *Ggcx*^{ff}*; Pdx1-Cre* islets and each mouse model was statistically significant for all comparisons and the highest significances were found for the comparison with islets from the diabetic mouse models (Table S3). Overall, these data suggest that loss of function of *Ggcx* in pancreatic endocrine cells induces a diabetic gene signature in these cells, presumably by altering their capacity to respond to ER stress.

GGCX is necessary for the maintenance of an adequate β-cell mass in adult mice

To determine the role of VK-dependent carboxylation in islet function in vivo, we next analyzed the metabolic consequences of a pancreas-specific inactivation of *Ggcx* (*Ggcx*^{ff}*; Pdx1-Cre* mice). The *Pdx1-Cre* driver was selected because it resulted in efficient deletion in pancreatic islets (Ferdaoussi et al., 2015), without expressing the human growth hormone (hGH), which was found to be present in several β-cell-specific Cre transgenes (*RIP-Cre*, *MIP-Cre*^{ERT}, etc.) and affect β-cell function and proliferation (Brouwers et al., 2014; Oropeza et al., 2015). *Ggcx* mRNA level was reduced by >90% and GGCX protein was undetectable in the pancreatic islets of these mice (Fig. S1E and Fig. 1F). In agreement with efficient inactivation of GGCX, protein γ-carboxylation was abrogated in *Ggcx*^{ff}*; Pdx1-Cre* islets (Fig. 1F). When compared to control littermates these mice did not display any differences in energy expenditure parameters (energy expenditure, O_2 consumption, CO_2 release), physical activity, food intake, pancreas weight and body weight (Fig. S2A-E). In addition, inactivation of *Ggcx* occurred only in the pancreas of the *Ggcx*^{ff}*; Pdx1-Cre* mice and not in any other tissue tested, including the hypothalamus and other parts of the brain (Fig. S2F).

Glucose tolerance test (GTT) revealed that an absence of γ-carboxylation in islets does not affect glucose handling in 16-weeks old mice (Fig. 3A). However, at 24 weeks of age, *Ggcx*^{ff}*; Pdx1-Cre* mice showed significantly elevated fasting blood glucose and decreased glucose tolerance (Fig. 3B). This defect could be traced to a reduction in glucose-stimulated insulin secretion (GSIS) (Fig. 3C), but not to reduced insulin sensitivity as assessed by an insulin tolerance test (Fig. 3D). Pancreas immunohistochemistry revealed that β-cell area and mass were reduced in *Ggcx*^{ff}*; Pdx1-Cre* mice at 32 weeks of age, but not at 12 weeks (Fig. 3E). Accordingly, total insulin content was diminished in the pancreas of 24-28 weeks old *Ggcx*^{ff}*; Pdx1-Cre* mice (Fig. 3F). Beta-cell area and β-cell mass were also

bioRxiv preprint doi: https://doi.org/10.1101/2022.05.13.491370; this version posted May 13, 2022. The copyright holder for this preprint (which was not certified by peer review) is the author/funder, who has granted bioRxiv a license to display the preprint in perpetuity. It is made available under aCC-BY-NC 4.0 International license.

significantly lower in mice lacking the two vitamin K oxidoreductases, *Vkorc1* and *Vkorc1l1*, in the pancreas only (Fig. S2G), confirming implication of the VK-cycle in the observed phenotype.

By western blot using antibodies against cleaved-caspase-3 and phospho(Ser139)-Histone H2A.X, we detected apoptosis and DNA damage in >32-weeks old *Ggcx^{ff}; Pdx1-Cre* islets, but not in *Ggcx^{ff}* controls (Fig. 3G). Beta-cell specific apoptosis was independently confirmed using TUNEL and insulin co-staining on pancreas sections (Fig. 3H). To rule out the possibility that the *Pdx1-Cre* transgene itself was responsible for the phenotype observed in *Ggcx^{ff}; Pdx1-Cre* mice, β-cell mass, β-cell apoptosis and pancreas insulin content were analyzed in *Pdx1-Cre* mice. None of these parameters were affected by the presence of the Cre recombinase (Fig. 3H and Fig. S2H-I). Altogether, our data suggest that GGCX and γ-carboxylation are necessary to maintain a proper β-cell mass and an adequate insulin response to glucose in aging mice.

Pancreas or β-cell specific deletion of *Ggcx* compromises insulin secretion in response to high fat diet

Because the phenotype of the *Ggcx^{ff}; Pdx1-Cre* mice appears to be age-dependent, we hypothesized that GGCX activity would be predominantly required when β-cells need to adapt to stress such as age-related insulin resistance. To test more directly GGCX involvement in acute β-cell stress response, 10-weeks old *Ggcx^{ff}; Pdx1-Cre* mice, which had not developed metabolic and β-cell mass phenotypes yet (Fig. 3A and 3E), were fed a high-fat diet (HFD; 60% kcal from fat) or a control low-fat diet (10% kcal from fat) for 7 days. Previous studies have established that one week of HFD feeding in mice was sufficient to induce β-cell ER stress, glucose intolerance and hyperinsulinemia, without significantly affecting peripheral insulin sensitivity (Sharma et al., 2015; Stamateris et al., 2013). qPCR analysis of ER-stress markers (*spliced Xbp1, Ddit3, Gadd34, Syvn1, Hspa5* and *Edem1*) on isolated islets confirmed that this short bout of HFD induces ER-stress in islets (Fig. S3A-F). This 7-day HFD feeding was also enough to increase body weight in mice, regardless of the presence of *Ggcx* in their islets (Fig. S3G). However, in contrast to control animals, mice deprived of *Ggcx* expression in islets were not able to maintain their fed blood glucose level following HFD (Fig. 4A). Insulin secretion in response to glucose in absolute value or expressed as a stimulation index (SI: blood insulin concentration at 15 minutes or 30 minutes over T0) was not affected in the absence of *Ggcx* in mice fed a control diet (Fig. 4B-C), in agreement with the fact that glucose handling was not altered in these mice at 12 weeks of age when fed a regular chow diet (Fig. 3A). In contrast, following 7 days on HFD,

bioRxiv preprint doi: https://doi.org/10.1101/2022.05.13.491370; this version posted May 13, 2022. The copyright holder for this preprint (which was not certified by peer review) is the author/funder, who has granted bioRxiv a license to display the preprint in perpetuity. It is made available under aCC-BY-NC 4.0 International license.

Ggcx^{ff}*; Pdx1-Cre* mice showed a strong suppression in SI, which was significantly lower than the SI of *Pdx1-Cre* control mice (Fig. 4D-E). Of note, this impaired glucose-stimulated insulin secretion in *Ggcx*^{ff}*; Pdx1-Cre* mice was associated with an elevated fasting insulin level (Fig. 4F), while fasting glucose was not reduced and glucose tolerance moderately impaired (Fig. S3H).

To determine if GGCX affects the capacity of β-cells to secrete insulin in a cell-autonomous manner, we next analyzed *Ggcx*^{ff}*; Ins-Cre* mice. At 10 weeks of age *Ggcx*^{ff}*; Ins-Cre* mice maintained on a regular chow diet had normal glucose tolerance, fasting glucose and fasting insulin (Fig. S3I-K). When *Ggcx*^{ff}*; Ins-Cre* mice were fed a HFD for 7 days, no difference in body weight was noted (Fig. S3L), but their fed glucose level was significantly increased (Fig. 4G) and their SI was reduced (Fig. 4H-I) in comparison to *Ins1-Cre* control mice. Remarkably, in the same animals, fasting insulin was significantly increased (Fig. 4J), although fasting glucose and glucose tolerance were respectively increased and unchanged (Fig. 4K and S3M). Fasting hyperglycemia associated with hyperinsulinemia suggests decreased peripheral insulin sensitivity in these animals. Together, these observations indicate that an absence of γ-carboxylation directly impacts β-cells' capacity to adapt their insulin secretion in the face of metabolic stress, resulting in increased fasting insulin and loss of glucose-stimulated insulin secretion.

To relate these findings to humans, we then analyzed *GGCX* and *VKORC1* gene expression in human islets from 15 non-diabetic and diabetic donors and observed that the level of these two enzymes vary widely between donors, but nevertheless strongly correlate with one another (Fig. 4L and Table S1). This observation suggests that for certain individuals, the γ-carboxylation machinery in their β-cells might be more active compared to others. Further analysis revealed that *GGCX* and *VKORC1* expression levels were positively correlated with the capacity of islets to secrete insulin in response to glucose (Fig. 4M-N), implying that γ-carboxylation could also impact glucose-stimulated insulin secretion in human β-cells.

Vitamin K attenuates apoptosis induced by ER calcium depletion

To determine if VK and γ-carboxylation can protect β-cells from the acute effects of ER stress, INS-1 832/3 β-cells were cultured for 24h in media containing 25mM glucose in the presence or absence of thapsigargin, an inhibitor of the sarco/endoplasmic reticulum Ca^{2+}-ATPase (SERCA), and a pharmacological inducer of ER stress (Sharma et al., 2015). At all doses tested, thapsigargin treatment

bioRxiv preprint doi: https://doi.org/10.1101/2022.05.13.491370; this version posted May 13, 2022. The copyright holder for this preprint (which was not certified by peer review) is the author/funder, who has granted bioRxiv a license to display the preprint in perpetuity. It is made available under aCC-BY-NC 4.0 International license.

stimulated protein γ-carboxylation only when VK_1 was included in the media (Fig. 4O). In addition, western blot experiments using antibodies against cleaved-caspase-3 and phospho(Ser139)-Histone H2A.X showed that thapsigargin dose-dependently induced apoptosis and DNA damage in β-cells, while pre-treatment with VK_1 reduced the deleterious effects of 10 and 20nM of thapsigargin in these cells (Fig. 4P). Together, these results suggest that γ-carboxylation is activated in response to ER stress to protect β-cells from apoptosis.

Gamma-carboxylation is increased in the islets of diabetes mouse models

To determine if γ-carboxylation is also activated in vivo in the context of β-cell ER stress, we next analyzed this enzymatic pathway in the islets of a series of diabetic animal models characterized by β-cell ER stress. *Ins2*$^{+/Akita}$ mice harbor a C96Y mutation in one of the murine insulin genes, preventing proper folding of pro-insulin, causing decompensated β-cell ER stress and diabetes (Riahi et al., 2018). Mice were analyzed at 7 weeks of age, after they developed symptoms of diabetes including hyperglycemia, hypoinsulinemia and polyuria (Fig. 5A-B). Gene expression analysis by qPCR revealed that both *Ggcx* and *Vkorc1* were significantly increased in islets from *Ins2*$^{+/Akita}$ mice (Fig. 5C). GGCX and VKORC1 protein levels were also elevated in *Ins2*$^{+/Akita}$ islets and the VK cycle was hyper-activated as indicated by the increased presence of multiple Gla proteins in these islet extracts (Fig. 5D). We also analyzed *Lepr*$^{db/db}$ mice on BKS background at 10 weeks of age when they are obese, hyperglycemic and polyuric (Fig. 5E-F) (Hummel et al., 1966). Similar to what was observed in *Ins2*$^{+/Akita}$ islets, *Lepr*$^{db/db}$ islets were characterized by increased GGCX and VKORC1 expression, and global protein γ-carboxylation (Fig. 5G-H). Finally, we performed the same analyses on 9-weeks old *Lep*$^{ob/ob}$ mice on C57BL/6J background. These mice develop obesity but are only transiently hyperglycemic (Fig. 5I-J) (Coleman and Hummel, 1973), and islets from these animals were also characterized by increased GGCX, VKORC1 and γ-carboxylation (Fig. 5K). Together these data suggest that GGCX, VKORC1 and γ-carboxylation are coordinately activated in vivo in conditions implicating β-cell adaptation to ER stress.

Glucose regulates vitamin K-dependent carboxylation in β-cells

Since hyperglycemia is a common feature of the *Ins2*$^{+/Akita}$, *Lepr*$^{db/db}$ and *Lep*$^{ob/ob}$ mouse models, we hypothesized that glucose itself could regulate the expression of the VK cycle enzymes and γ-carboxylation in β-cells. We therefore cultured wild type C57BL/6J mouse islets for 3 days in media containing either 5 or 15mM glucose and assessed the impact on GGCX and VKORC1 expression and

bioRxiv preprint doi: https://doi.org/10.1101/2022.05.13.491370; this version posted May 13, 2022. The copyright holder for this preprint (which was not certified by peer review) is the author/funder, who has granted bioRxiv a license to display the preprint in perpetuity. It is made available under aCC-BY-NC 4.0 International license.

VK cycle function. We observed that *Ggcx* and *Vkorc1* expression was increased both at the mRNA and protein level in response to 15mM glucose (Fig. 5L-M). GGCX expression and γ-carboxylation were also induced when the rat β-cell line INS-1 832/3 was grown in presence of high glucose (25 mM) concentrations (Fig. 5N). To confirm that glucose regulates the VK cycle in vivo, 2-month-old Wistar rats were infused with glucose for 3 days, had their islets isolated and gene expression was analyzed by qPCR. Glycemia reached ~15 mM in glucose-infused rats (Fig. 5O), and this was sufficient to significantly increase *Ggcx* and *Vkorc1* expression in their islets (Fig. 5P) compared to rats infused with saline solution which maintained their blood glucose at ~7 mM. Finally, GGCX expression and global γ-carboxylation were also increased in non-diabetic human islets cultured for 3 days in media containing 15mM glucose compared to islets cultured with 5mM glucose (Fig. 5Q, Table S1).

Junctate is a vitamin K-dependent carboxylated protein expressed in β-cells

To elucidate the molecular mechanism by which VK-dependent carboxylation regulates β-cell survival and insulin secretion, we next sought to identify γ-carboxylated protein(s) present in β-cells. In our mouse islet RNAseq dataset, genes encoding for known γ-carboxylated proteins including the clotting factors II, VII, IX and X, matrix Gla protein and osteocalcin were all expressed at very low level (Fig. S4A). Together with the detection in islets of multiple γ-carboxylated proteins by western blot (Fig. 1F), these observations suggest that β-cells express previously uncharacterized Gla proteins. In the context of another project, we immunoprecipitated γ-carboxylated proteins from 5-day old wildtype (WT) mouse liver extracts using our pan-specific α-Gla antibody and identified by mass spectrometry aspartyl/asparaginyl β-hydroxylase (ASPH) as a novel putative intracellular Gla protein (Table S4). The *Asph* gene undergoes extensive alternative splicing and encodes for multiple ER-resident proteins including ASPH, junctate and junctin (Feriotto et al., 2005) (Fig. S4B). ASPH is a type II transmembrane protein of ~110 kDa containing three luminal domains: an EF-hand calcium-binding domain, a negatively charged Glu rich domain (GRD) containing 39 Glu residues, and an alpha-ketoglutarate dependent hydroxylase domain. Junctate is an ER-resident protein of ~50-55 kDa and is identical to ASPH but lacks the hydroxylase domain. The N-terminus of junctin is identical to junctate, but instead of a GRD, its C-terminus is composed of a positively charged lysine-rich domain. Our RNAseq data indicates that overall *Asph* expression level in islets is comparable to *Ggcx* and higher than any of the other genes encoding for known γ-carboxylated proteins (Fig. S4A). Moreover, the mRNAs encoding for ASPH and junctate isoforms are both expressed in pancreatic islets, with junctate mRNA being at least three times more expressed than ASPH mRNA (Fig. S4B-C). Junctin mRNA was

bioRxiv preprint doi: https://doi.org/10.1101/2022.05.13.491370; this version posted May 13, 2022. The copyright holder for this preprint (which was not certified by peer review) is the author/funder, who has granted bioRxiv a license to display the preprint in perpetuity. It is made available under aCC-BY-NC 4.0 International license.

not detected in mouse pancreatic islets (Fig. S4B-C). We thus decided to determine if ASPH and junctate were the γ-carboxylated proteins detected in islets and β-cells.

ASPH (A) and junctate (J), but not junctin, share a GRD that could be prone to γ-carboxylation. To detect specifically these two proteins, we generated and affinity-purified rabbit polyclonal antibodies against the GRD domain; hereafter called α-A/J-GRD. Western blot analysis showed that these antibodies cannot detect ASPH or junctate deletion mutants that do not possess the GRD (Fig. S4D-E). Importantly, the addition of either VK_1 or warfarin did not change the immunoreactivity of α-A/J-GRD antibodies towards full-length ASPH and junctate, suggesting that γ-carboxylation does not impact α-A/J-GRD binding (Fig. S4E). Anti-Gla immunoprecipitation (IP) followed by α-A/J-GRD western blot or α-A/J-GRD IP followed by α-Gla western blot, allowed us to confirm that both ASPH and junctate are γ-carboxylated in one-week-old WT liver, but not in the liver of *Vkorc1*$^{-/-}$ mice lacking γ-carboxylation at this age (Fig. S4F-G) (Lacombe et al., 2018). Using the same approach, we could show that ASPH and junctate are expressed and γ-carboxylated in adult control mouse islets, and that their γ-carboxylation was greatly reduced in islets isolated from *Vkorc1*$^{-/-}$;*APOE-Vkorc111*^{73} mice, which have lower VK oxidoreductase activity and γ-carboxylation in all tissues except the liver (Fig. 6A and Fig. S4H) (Lacombe et al., 2018). Interestingly, these analyses showed that junctate expression and γ-carboxylation were respectively ~7 and 8-fold higher than ASPH in control islets (Fig. 6A-B and Fig. S4H). In addition, junctate γ-carboxylation was significantly increased in *Ins2*$^{+/Akita}$ diabetic islets compared to non-diabetic islets, while γ-carboxylated ASPH was barely detectable regardless of the genotype (Fig. 6C). The expression of both ASPH and junctate was increased in *Ins2*$^{+/Akita}$ islets in western blot analyses (Fig. 6C), and immunofluorescence confirmed the β-cell expression of these proteins in non-diabetic and diabetic β-cells (Fig. 6D-E). Together these results establish that junctate, and to a lower extent ASPH, are novel γ-carboxylated proteins expressed in mouse β-cells.

Junctate is γ-carboxylated on several glutamic acid residues located in its Glu-rich domain

To identify the domain(s) and specific glutamic acid residues subjected to γ-carboxylation in ASPH and junctate, we first expressed full-length ASPH-3XFLAG, or mutants lacking either the cytosolic, the EF-hand or the Glu-rich domain in HEK293 cells (Fig. S4D), which support VK-dependent carboxylation (Lacombe et al., 2018). Full-length ASPH γ-carboxylation was detected in HEK293 cells cultured in presence of VK_1, but not in presence of warfarin (Fig. S4I). Although neither deletion of the

bioRxiv preprint doi: https://doi.org/10.1101/2022.05.13.491370; this version posted May 13, 2022. The copyright holder for this preprint (which was not certified by peer review) is the author/funder, who has granted bioRxiv a license to display the preprint in perpetuity. It is made available under aCC-BY-NC 4.0 International license.

cytosolic nor the EF-Hand domains significantly affected ASPH γ-carboxylation, deletion of the GRD completely abrogated its γ-carboxylation (Fig. S4I). The amino acid sequence of the GRD is poorly conserved across mammalian species. However, the enrichment of glutamic acid residues has been retained throughout evolution, suggesting a fundamental biological function for ASPH/junctate GRD γ-carboxylation (Fig. S4J). Internal deletions within the GRD of junctate indicated that most of the γ-carboxylation sites are in the region encompassing residues 255 to 310 and/or that the C-terminal domain contains a critical sequence for the recognition by GGCX (Fig. 6F-G). To rule out the possibility that this deletion reduces γ-carboxylation by affecting junctate conformation and recognition by GGCX, we mutated glutamic acid residues throughout the GRD into aspartic acid residues, which cannot be γ-carboxylated by GGCX (Fig. 6F). Using this series of mutant proteins, we found that γ-carboxylated residues are mainly located in the N- and C-terminal regions of the GRD (Fig. 6H-I and Fig. S4K). In agreement with these findings, LC-MS/MS analysis detected the presence of γ-carboxylated residues at the N- and C-terminus of the GRD (Fig. 6J-K and Table S5). Confirming the specificity of this LC-MS/MS approach, no Gla containing peptides were identified when junctate was purified from HEK293 cells treated with warfarin or from E. coli which lack γ-carboxylation machinery (Fig. 6K). Human junctate expressed in HEK293 cells was also γ-carboxylated in a VK-dependent manner (Fig. S4L).

Junctate γ-carboxylation regulates calcium flux in β-cells.

Since our data suggest that junctate is the predominant γ-carboxylated protein present in islets and β-cells, we decided to further investigate the role of junctate in these cells. Junctate's GRD was previously shown to bind free calcium ions (Ca^{2+}) (Treves et al., 2000) and γ-carboxylation increases the affinity of proteins for Ca^{2+} (Furie et al., 1999). Therefore, we next tested whether this post-translational modification could modulate the calcium-binding capacity of junctate. Carboxylated and uncarboxylated junctate-3XFLAG were expressed and purified from HEK293 cells cultured in the presence of VK_1 or warfarin respectively (Fig. 7A). As revealed by $^{45}Ca^{2+}$ overlay experiments, γ-carboxylated junctate binds significantly more calcium than its uncarboxylated counterpart when identical amounts of protein were used in the assay (Fig. 7B-C), suggesting that the presence of Gla residues in the GRD increases junctate capacity to bind Ca^{2+}.

Junctate has previously been implicated in ER-cytosol calcium homeostasis through interaction with Stromal interaction molecule 1 (STIM1) and the IP3 receptor (IP3R) (Srikanth et al., 2012; Treves et

bioRxiv preprint doi: https://doi.org/10.1101/2022.05.13.491370; this version posted May 13, 2022. The copyright holder for this preprint (which was not certified by peer review) is the author/funder, who has granted bioRxiv a license to display the preprint in perpetuity. It is made available under aCC-BY-NC 4.0 International license.

al., 2004). A study in T cells suggested that junctate acts as a calcium-sensing ER protein regulating the STIM1-Orai1 protein complex (Srikanth et al., 2012), which is critical to activate store-operated calcium entry (SOCE), a cellular response whereby extracellular calcium enters the cytosol following ER calcium depletion. Importantly, SOCE has been implicated in insulin secretion from β-cells (Sabourin et al., 2015), with loss of STIM1 leading to reduced insulin secretion and increased ER stress (Kono et al., 2018). These observations prompted us to investigate whether junctate γ-carboxylation would affect cellular calcium flux and SOCE.

To eliminate potential confounding effects caused by endogenous human ASPH or junctate, we used CRISPR/Cas-9 genome editing to knockout ASPH and junctate in HEK293 cells (*Asph/Junctate*$^{-/-}$ HEK293) (Fig. S5A-B). Store-operated calcium entry (SOCE) machinery was recapitulated in these cells by expressing STIM1-Myc and Orai1-HA, in presence or absence of junctate-3XFLAG. Cells were then cultured with or without VK_1 to modulate junctate carboxylation (Fig. 7D). Carboxylated GGCX was detected in VK_1 treated cells regardless of junctate expression, confirming efficient γ-carboxylation in these cells. Cytosolic calcium measurement by live-cell imaging using the calcium indicator Fluo-4 was next used to assess SOCE, which was triggered first by depleting ER calcium with thapsigargin in Ca^{2+} free buffer followed by calcium addback to the buffer (Fig. 7E). Using this experimental setting, we observed that cells expressing carboxylated junctate are characterized by a diminution in their ER calcium release as well as reduced SOCE, suggesting that junctate, only when γ-carboxylated, restrains cytosolic calcium flux in cells (Fig. 7F-H).

STIM1 is an ER transmembrane protein that acts as a calcium sensor, which upon ER calcium depletion is transported to plasma membrane (PM) proximal ER puncta where it oligomerizes and triggers heteromerization with the plasma membrane calcium channel Orai1 at these puncta (Lunz et al., 2019). Activation of SOCE in cells is therefore characterized by the formation of ER-PM junction puncta containing both STIM1 and Orai1, as observed following a 15 minutes thapsigargin treatment (Fig. 7I). In these conditions, VK_1 or junctate alone did not affect the formation of STIM1-Orai1 puncta, but the presence of γ-carboxylated junctate significantly reduced the formation of these protein complexes (Fig. 7I-J and Fig. S5C-D). We also observed that junctate, regardless of its γ-carboxylation status, co-localizes with STIM1 in untreated cells (Fig. S5E-F). However, following SOCE activation, uncarboxylated junctate and STIM1 localization are mutually exclusive, while γ-carboxylated junctate colocalizes with STIM1 outside STIM1-containing puncta (Fig. S5E-F). These results suggest that

bioRxiv preprint doi: https://doi.org/10.1101/2022.05.13.491370; this version posted May 13, 2022. The copyright holder for this preprint (which was not certified by peer review) is the author/funder, who has granted bioRxiv a license to display the preprint in perpetuity. It is made available under aCC-BY-NC 4.0 International license.

when γ-carboxylated, junctate may sequester STIM1 in the ER and limit the formation of STIM1-Orai1 complexes, thus restraining SOCE.

Analysis of islets lacking *Ggcx* activity exclusively in β-cells revealed that junctate, but not ASPH, is γ-carboxylated in β-cells (Fig. 7K). Therefore, we next used *Ggcx*^{ff}*; Ins-Cre* islets as a genetic model of decarboxylated junctate in β-cells to determine how γ-carboxylation of this protein affects calcium homeostasis in these cells. Cytosolic calcium flux was analyzed in partially dissociated islet cells from *Ggcx*^{ff}*; Ins-Cre* and *Ins1-Cre* (control) mice by ratiometric live-cell imaging using the Fluo-4 and Fura-Red Ca^{2+} indicators. First, we monitored SOCE and observed that *Ggcx*^{ff}*; Ins-Cre* β-cells lacking γ-carboxylated junctate are characterized by higher cytosolic calcium levels at baseline and during SOCE, but normal ER calcium release (Fig. 7L-N and Fig. S5G). Second, we measured calcium flux in response to glucose and confirmed higher basal cytosolic calcium levels in *Ggcx*^{ff}*; Ins-Cre* islets in comparison to *Ins1-Cre* islets. However, cytosolic calcium levels after stimulation with 15mM glucose or KCl were unchanged in absence of carboxylated junctate when normalized over the baseline, although they remained elevated in absolute value (Fig. 7O-Q). Altogether, these data suggest that junctate γ-carboxylation is necessary to maintain calcium homeostasis in β-cells, mainly by suppressing SOCE (Fig. 7R).

bioRxiv preprint doi: https://doi.org/10.1101/2022.05.13.491370; this version posted May 13, 2022. The copyright holder for this preprint (which was not certified by peer review) is the author/funder, who has granted bioRxiv a license to display the preprint in perpetuity. It is made available under aCC-BY-NC 4.0 International license.

DISCUSSION

Clinical studies previously suggested that VK insufficiency or reduced VK intake is associated with an increased risk of developing diabetes and that VK supplementation can improve glycemia in patients with diabetes. However, the precise molecular mechanism by which VK might protect from T2D, including the tissue(s) and the protein(s) involved has never been addressed. In this study, we establish that VK-dependent carboxylation is present in β-cells and that inactivation of this pathway specifically in the pancreas or β-cells impairs the capacity of these cells to adapt to metabolic stress. We also identified junctate as a novel γ-carboxylated protein present in β-cells and provide evidence that this protein regulates intracellular calcium in a carboxylation-dependent manner. Altogether, our work identified a previously undescribed function of γ-carboxylation in the regulation of β-cell function, providing the basis for a potential molecular and cellular mechanism by which VK may protect from T2D.

Link between the VK-cycle and metabolic stress in β-cells

VK-dependent carboxylation was previously shown to play a critical role in the liver, where it is essential for the activation of a series of coagulation factors and in arteries, cartilage, and bone where it controls the activity of two small Gla proteins: MGP and osteocalcin. Here, using conditional inactivation of *Ggcx* in mice and unique α-Gla antibodies, we establish for the first time that the VK cycle is active in pancreatic islets and, more specifically, in β-cells.

In addition, we observed a hyper-activation of the VK cycle in islets isolated from three different mouse models characterized by stressed β-cells. *B6-Lep*$^{ob/ob}$ mice in contrast to *BKS-Lepr*$^{db/db}$ mice do not develop diabetes due to the capacity of their β-cells to adapt to insulin resistance (Clee et al., 2006), yet both models displayed increased islet γ-carboxylation. These observations suggest that hyper-activation of the VK cycle is not a mere non-specific consequence of diabetes, but most likely a compensatory mechanism activated during β-cell adaptation to stress. Further supporting a link between γ-carboxylation and β-cell adaptation to ER stress, we found that a large set of genes was similarly dysregulated in *Ggcx*-deficient islets and in islets isolated from pre-diabetic and diabetic mice. Moreover, GGCX and γ-carboxylation were induced ex vivo in islets or in INS-1 832/3 β-cells when cultured with high glucose concentrations, a condition known to induce mild ER stress in β-cells (Sharma et al., 2015). Finally, γ-carboxylation was further induced in INS-1 832/3 β-cells when they were exposed to low doses of thapsigargin in combination with high glucose, and γ-carboxylation

bioRxiv preprint doi: https://doi.org/10.1101/2022.05.13.491370; this version posted May 13, 2022. The copyright holder for this preprint (which was not certified by peer review) is the author/funder, who has granted bioRxiv a license to display the preprint in perpetuity. It is made available under aCC-BY-NC 4.0 International license.

partially protected these cells from ER stress-induced apoptosis. These data, together with the observation that the mice lacking *Ggcx* in pancreas or in β-cell only failed to adapt their insulin secretion in response to a short HFD feeding, suggest that the VK cycle could be part of a compensatory mechanism implicated in β-cell survival and function (Fig. 7R).

Junctate γ-carboxylation as a regulator of β-cell calcium homeostasis

Our results identified junctate as a previously unrecognized γ-carboxylated protein present in islets and β-cells. We also establish that junctate γ-carboxylation increases by several folds in diabetic mouse islets and β-cells. Based on these observations and on a previously reported role for this protein in ER-cytosol calcium homeostasis and SOCE, we investigated the effect of junctate γ-carboxylation on cellular calcium flux. Our data show that γ-carboxylated junctate reduces the formation of STIM1 and Orai1 puncta following ER calcium store depletion in agreement with partial SOCE inhibition. Decarboxylated junctate did not have any effect on puncta formation or SOCE in this heterologous cell system lacking endogenous junctate. Conversely, decarboxylation of junctate in *Ggcx*^{ff}*; Ins-Cre* β-cells was associated with an increase in cytosolic calcium level at baseline and following SOCE. Others have reported that junctate also interacts with and regulates the sarco-endoplasmic reticulum Ca^{2+}-ATPase 2 (SERCA2) pump and the inositol 1,4,5 trisphosphate receptors (IP3R), two other ER membrane proteins controlling calcium flux between the ER and the cytosol (Kwon and Kim, 2009; Treves et al., 2004). It is important to note however, that in these earlier publications junctate was studied in its decarboxylated form, since VK was not included in the culture media. Thus, we cannot exclude, at this point, that carboxylated junctate also regulates calcium homeostasis in β-cell through SERCA2 or IP3R.

STIM1 and SOCE have previously been shown to positively regulate insulin secretion and to reduce ER stress in β-cells (Kono et al., 2018; Sabourin et al., 2015). Other studies have shown that alteration in either ER or cytosolic free calcium levels can induce ER stress and β-cell death (Sabatini et al., 2019). In addition, the expression level and the activity of STIM1 and SERCA2 were found to be reduced in human or mouse T2D islets, and to correlate with altered cytosolic calcium in response to glucose (Kono et al., 2018; Liang et al., 2014). In line with these findings, it was recently reported that tunicamycin-induced ER stress decreases ER calcium levels and increases SOCE in β-cells resulting in increased basal insulin secretion (Zhang et al., 2020). Overall, this body of literature suggests that the short-term activation of calcium flux between ER and cytosol and of SOCE is critical for several β-cell

bioRxiv preprint doi: https://doi.org/10.1101/2022.05.13.491370; this version posted May 13, 2022. The copyright holder for this preprint (which was not certified by peer review) is the author/funder, who has granted bioRxiv a license to display the preprint in perpetuity. It is made available under aCC-BY-NC 4.0 International license.

cellular processes including survival and insulin secretion, but that chronic stimulation of calcium signaling pathway can induce ER stress, β-cell dysfunction and death (Sabatini et al., 2019). Our data show that the Ca^{2+} binding capacity of junctate increases when γ-carboxylated and that this modification restrains SOCE. This process appears to be necessary to maintain appropriate cytosolic calcium levels in β-cells, suggesting a model where γ-carboxylated junctate would act as an ER Ca^{2+} sensor. Under conditions of chronically elevated intracellular calcium levels, reducing Ca^{2+} entry would prove beneficial to prevent β-cell dysfunction and diabetes progression. As noted above, the increased level of γ-carboxylated junctate observed in diabetic mouse islets may therefore be a compensatory mechanism activated in response to sustained elevated glucose in an effort of the β-cell to restore appropriate calcium level and preserve its function (Fig. 7R). In humans, insufficient VK intake may therefore contribute to β-cell dysfunction in condition of β-cell stress by reducing junctate γ-carboxylation, thereby increasing the risk of T2D.

Noteworthily, the mice lacking GGCX in the pancreas or only in β-cells and fed a HFD for 7 days are characterized not only by a reduced glucose-stimulated insulin secretion and increased blood glucose, but also by an increased fasting serum insulin. These observations are consistent with the notion that in condition of nutrient excess, chronic elevation of intracellular calcium and ER stress in β-cells can lead to uncontrolled hyperinsulinemia which could ultimately result in peripheral insulin resistance (Yong et al., 2021). There is a growing number of studies in rodents and humans suggesting that prolonged fasting insulin hypersecretion precedes and promotes insulin resistance and could be the initiating event of T2D (Hudish et al., 2019; Mittendorfer et al., 2022). Conversely, reducing insulin secretion can prevent insulin resistance, obesity, and fatty liver disease (Mehran et al., 2012; Yong et al., 2021). The metabolic phenotype of the *Ggcx*^{ff}*; Ins-Cre* mice following a short period of HFD suggests that γ-carboxylated junctate may be required both to prevent uncontrolled insulin secretion by β-cells in the context of nutrient excess and to preserve normal glucose-stimulated insulin secretion.

Junctate as a novel VK-dependent protein

Since the discovery more than 45 years ago that a group of clotting factors was γ-carboxylated on specific glutamic acid residues in a VK-dependent manner (Stenflo et al., 1974), a total of only 15 unique Gla proteins have been identified in mammals. They all share a relatively well-conserved "Gla domain" characterized by the presence of 3 to 12 γ-carboxylated glutamic acid residues and two cysteines forming a disulfide bridge. Here, we identify junctate and ASPH as two previously

bioRxiv preprint doi: https://doi.org/10.1101/2022.05.13.491370; this version posted May 13, 2022. The copyright holder for this preprint (which was not certified by peer review) is the author/funder, who has granted bioRxiv a license to display the preprint in perpetuity. It is made available under aCC-BY-NC 4.0 International license.

unrecognized Gla proteins in liver and β-cells. The presence of Gla residues in the GRD of junctate was confirmed with two independent approaches: detection with previously reported Gla-specific antibodies and LC-MS/MS. These observations were also validated in genetic models lacking either *Ggcx* or *Vkorc1*. The GRD domain of junctate was previously described as a calcium-binding domain (Treves et al., 2000) and our data indicate that the presence of Gla residues in the GRD further increases its capacity to bind calcium in vitro.

The GRD domain of junctate/ASPH possesses several unique features compared to the classical Gla proteins. First, junctate and ASPH are ER-resident proteins, while the other known Gla proteins are either secreted or plasma membrane proteins. Second, the ASPH/junctate GRD, with more than 190 amino acids (a.a.), is larger than the classical Gla domains which are on average less than 50 a.a. long. In addition, the sequence of the GRD is not similar in any way to the other Gla proteins, except for the presence of multiple Glu residues. Third, in contrast to the classical Gla domain, the ASPH/junctate GRD does not contain a disulfide bridge and the Gla residues are distributed in the N- and C-terminal regions instead of being clustered in the center. Fourth, junctate and ASPH do not contain a sequence matching the GGCX substrate recognition sequence found in the other Gla proteins. Together with the observation that GGCX itself is also γ-carboxylated and lacks such a substrate recognition sequence (Hallgren et al., 2013), it suggests that GGCX can recognize substrates through at least two different mechanisms.

Several non-vertebrate metazoans, including insects and mollusks, possess in their genome genes encoding for GGCX and VKORC1 homologues (Bandyopadhyay et al., 2002). Yet, homologues for the known vertebrate Gla proteins are not present in these organisms, suggesting that the ancestral function(s) and wider biological roles of γ-carboxylation still need to be defined. Genome database searches allowed us to identify ASPH/junctate homologues containing a GRD in several of these non-vertebrate metazoans possessing a GGCX homologue (data not shown). These observations suggest that regulation of ER-cytosolic calcium homeostasis through junctate γ-carboxylation could be an evolutionarily conserved mechanism, which antedates divergence of mollusks, arthropods, and vertebrates.

In conclusion, we identify here VK-dependent γ-carboxylation as an important post-translational modification present in β-cells which regulates the capacity of these cells to adapt to stress. We also

bioRxiv preprint doi: https://doi.org/10.1101/2022.05.13.491370; this version posted May 13, 2022. The copyright holder for this preprint (which was not certified by peer review) is the author/funder, who has granted bioRxiv a license to display the preprint in perpetuity. It is made available under aCC-BY-NC 4.0 International license.

identified two new mammalian VK-dependent proteins, junctate and ASPH, and provide evidence that γ-carboxylation may regulate β-cell calcium homeostasis through junctate. Together, our findings extend the cellular and physiological function of VK-dependent γ-carboxylation and reveal how this pathway may interact with the development of diabetes.

ACKNOWLEDGEMENTS

We thank C. Julien and D. Pham for mouse genotyping and cell maintenance, Dr K. Suh for providing the B6.Cg-*Gt(ROSA)26Sor*$^{tm14(CAG\text{-}tdTomato)Hze}$/J mice, Dr V. Calderon for RNA-Seq analysis and Dr. G. Karsenty for his critical reading of the manuscript. We also thank the staff of IRCM Proteomics, Microscopy, Molecular Biology and Histology Core Facilities for their technical support. We thank Dr. P.E. MacDonald and the Alberta Diabetes Institute IsletCore for human islets isolation and are indebted to organ donors and their families for their generous support of scientific research. This work was supported by funding from the Canada Research Chair program (MF), Diabetes Canada (MF), the Canadian Institutes of Health Research (MF, PJT-169685 and PJT-175025; VP, MOP-77686), the US National Institutes of Health (VP, R01-DK-58096) and the CMDO Network (MF). KG received scholarships from IRCM and the Natural Sciences and Engineering Research Council of Canada. JL received a fellowship from Diabetes Canada.

Author contributions

J.L. and M.F. conceived the study, designed the experiments, and initiated the project. J.L., K.G., D.F. and M.F. collected and analyzed data. J.S., F.G., S.M.M., and S.H. collected data. A.V. and V.P. prepared cDNA from islets mRNA isolated from rats perfused with glucose or saline. M.F. and J.L. wrote the manuscript and all authors commented and contributed to editing the final version. M.F. acts as the guarantor of this work and is responsible for data access. J.L. is listed before K.G. as co–first author because J.L. conceived the study, designed the experiments, and wrote the manuscript.

Declaration of interests

The authors declare no conflict of interests.

bioRxiv preprint doi: https://doi.org/10.1101/2022.05.13.491370; this version posted May 13, 2022. The copyright holder for this preprint (which was not certified by peer review) is the author/funder, who has granted bioRxiv a license to display the preprint in perpetuity. It is made available under aCC-BY-NC 4.0 International license.

FIGURE LEGENDS

Figure 1: Vitamin K-dependent carboxylation machinery is active in islets and β-cells. (A) GGCX and VKORC1 protein abundance in various human tissues expressed as normalized intensity based absolute quantification (iBAQ; www.proteomicsdb.org). **(B-C)** Dispersed islet cells from *Ins1*$^{Cre/+}$;*Rosa26*$^{CAG\text{-}lox\text{-}stop\text{-}lox\text{-}tdTomato}$ mice were sorted by flow cytometry based on tdTomato expression (Tom+ versus Tom-) and gene expression analysed by quantitative PCR and normalized to *Actb* (n=3; mean ± SEM; unpaired, 2-tailed Student's *t* test; ***$P < 0.001$; *$P < 0.05$). **(D)** Protein expression in β-cells, islets and livers from *Ins1*$^{Cre/+}$;*Rosa26*$^{CAG\text{-}lox\text{-}stop\text{-}lox\text{-}tdTomato}$ mice was measured by western blot using anti-Gla, anti-GGCX and anti-VKORC1 antibodies. β-Actin was used as a loading control. **(E)** INS-1 832/3 cells were cultured in presence of vitamin K_1 (VK_1; 22μM) or vehicle for 3 days and GGCX γ-carboxylation was assessed by anti-Gla immunoprecipitation followed by western blot analysis with α-GGCX antibodies. **(F)** Islets from *Ggcx*^{ff}, *Pdx1-Cre* and *Ggcx*^{ff}*; Ins1-Cre* mice and their respective *Ggcx*^{ff} littermates were harvested and γ-carboxylation and GGCX expression were analysed by western blot using anti-Gla and anti-GGCX antibodies. β-actin was used as a loading control. Arrows indicate carboxylated proteins, while asterisks indicate non-specific binding. **(G)** Human islets from a non-diabetic cadaveric donor (R266) were cultured in presence of VK_1 (22μM), warfarin (50μM) or vehicle for 48h and γ-carboxylation and GGCX expression were analysed by western blot using anti-Gla and anti-GGCX antibodies. β-actin was used as a loading control.

Figure 2: Absence of *Ggcx* induces a diabetic signature in islets. (A-C) Gene expression in *Ggcx*^{ff}*; Pdx1-Cre* and *Ggcx*^{ff} islets were analyzed by bulk RNA-sequencing and gene set enrichment analysis was performed for genes significantly modulated by *Ggcx* (false discovery rate (FDR) ≤ 0.05) using the **(A)** Gene Ontology (GO) biological processes terms, **(B)** KEGG pathways and **(C)** Keywords in the Uniprot database. Data are represented as $-\log_{10}$(FDR) and the number of genes associated to each pathway is indicated on the bar graphs. **(D)** Schematic representing a protein-protein interaction network associated to endoplasmic reticulum protein processing and response to stress, within the differentially expressed gene set (analyzed using StringDB). **(E)** Venn diagram representing the overlap between the transcriptome of *Ggcx*^{ff}*; Pdx1-Cre* islets and islets from pre-diabetic (HFD for 8 weeks) or diabetic (*Lepr*$^{db/db}$ and *Ire1α*$^{\beta\text{-}/\text{-}}$) mouse models. The top panel represents the overlap between the significantly up-regulated genes in all models, while the bottom panel represents the down-regulated genes. Number of genes is shown for each overlap. **(F)** Heat map representing 198 genes

bioRxiv preprint doi: https://doi.org/10.1101/2022.05.13.491370; this version posted May 13, 2022. The copyright holder for this preprint (which was not certified by peer review) is the author/funder, who has granted bioRxiv a license to display the preprint in perpetuity. It is made available under aCC-BY-NC 4.0 International license.

dysregulated in *Ggcx*-deficient islets and in the islets of at least one of 3 mouse models of diabetes or pre-diabetes (HFD, *db/db* and *Ire1*$^{\beta-/-}$). Genes were next clustered according to enrichment for UniProt keywords (Glycoproteins, Plasma membrane, Signal secreted), Gene Ontology biological process (Response to ER stress) or KEGG pathway (NFkappa B and TNF signaling pathway).

Figure 3: *Ggcx* is essential to the acquisition of an appropriate β-cell mass. (A-B) Glucose tolerance test (GTT) with *Ggcx*^{ff}*; Pdx1-Cre* and *Ggcx*^{ff} male mice was performed following an over-night fast and intra-peritoneal injection of a bolus of glucose (2g/kg of body weight). Blood glucose was analyzed at fasting and at 15, 30, 60 and 120 minutes post-injection in **(A)** 16-weeks-old (n=16-21) and **(B)** 24-weeks-old (n=15-23) mice. **(C)** Glucose stimulated insulin secretion (GSIS) was measured after an over-night fast and intra-peritoneal injection of a bolus of glucose (3g/kg of body weight) in 24-weeks-old male mice (n=10). Serum was collected at fasting and 15 and 30 minutes post-injection and insulin concentration measured by ELISA. **(D)** Insulin tolerance test (ITT) was performed following a 4h fast and intra-peritoneal injection of insulin (1U/kg) in 24-weeks-old male mice (n=9-10). **(E)** Histomorphometric analysis on pancreas section following insulin staining and hematoxylin counterstaining from 12- and 32-weeks-old mice (n=10-11). **(F)** Pancreas from 24- to 28-weeks old *Ggcx*^{ff}*; Pdx1-Cre* and *Ggcx*^{ff} male mice were homogenized and insulin content measured by ELISA (n=8). **(G)** The presence of cleaved-caspase-3 and p(Ser139)-Histone H2A.X in *Ggcx*^{ff}*; Pdx1-Cre* and *Ggcx*^{ff} islets was analysed by western blotting. β-Actin was used as a loading control. **(H)** β-cell specific apoptosis was detected by TUNEL and insulin co-staining on pancreas sections from 32-weeks old mice. Results represent the mean ± SEM. Two-way ANOVA with Bonferroni's post tests were used for repeated measurements; ordinary one-way ANOVA was used for multiple comparisons and unpaired, two-tailed Student's *t* test was used for simple comparison; $^{**}P < 0.01$; $^{*}P < 0.05$.

Figure 4: Gamma-carboxylation is necessary for β-cell function and survival. (A-L) Ten-weeks old male mice of different genotypes were fed with a high-fat (60%) or a control low-fat (10%) diet for 7 days and metabolic analysis performed. **(A)** Fed blood glucose level of *Ggcx*^{ff}*; Pdx1-Cre* and *Ggcx*^{ff} male mice (n=4-6). **(B-C)** For the control low-fat diet fed *Ggcx*^{ff}*; Pdx1-Cre* and *Ggcx*^{ff} mice, glucose stimulated insulin secretion (GSIS) was measured after a 5-hour fast and intra-peritoneal injection of a bolus of glucose (2g/kg of body weight) (n=8-13). Data are represented in **(B)** absolute value and **(C)** as stimulation index (blood insulin concentration at 15 or 30 minutes over T0). The dashed line represents a stimulation index of 1 at fasting. **(D-F)** For the high-fat diet fed *Ggcx*^{ff}*; Pdx1-Cre, Ggcx*^{ff}

bioRxiv preprint doi: https://doi.org/10.1101/2022.05.13.491370; this version posted May 13, 2022. The copyright holder for this preprint (which was not certified by peer review) is the author/funder, who has granted bioRxiv a license to display the preprint in perpetuity. It is made available under aCC-BY-NC 4.0 International license.

and *Pdx1-Cre* mice, GSIS are represented in **(D)** absolute value or **(E)** as stimulation index**,** and **(F)** fasting insulin levels are shown (n=8-21). **(G-L)** Metabolic analysis of *Ggcx*^{ff}*; Ins1-Cre* and *Ins1-Cre* mice following 7 days HFD feeding. **(G)** Fed blood glucose, **(H-I)** GSIS, **(J)** fasting insulin and **(K)** fasting blood glucose were measured (n=10-12). Results represent the mean ± SEM. Two-way ANOVA with Bonferroni's post tests were used for repeated measurements, ordinary one-way ANOVA was used for multiple comparisons and unpaired two-tailed Student's *t* test was used for simple comparison; $^{**}P < 0.01$; $^{*}P < 0.05$. **(L-N)** Correlation in 15 human islet donor samples between **(L)** *Ggcx* and *Vkorc1* gene expression levels, and between **(M)** *Ggcx* or **(N)** *Vkorc* and each sample's stimulation index (insulin secretion at 10mM over 1mM glucose). Data were normalized using *Actb* and association were analyzed using Pearson's correlation. Black circles represent non-diabetic male donors, red circles diabetic male donors, black triangle non-diabetic female donor and red triangle diabetic female donor. **(O-P)** INS-1 832/3 cells were cultured with VK_1 (22μM) or vehicle for 48 hours before being cultured for 24 hours in media containing 25mM glucose and thapsigargin (0, 10, 20, 40nM). Western blot was performed to analyze **(O)** γ-carboxylation using anti-Gla antibodies, and **(P)** cellular fitness using cleaved-caspase-3 and p(Ser139)-Histone H2A.X antibodies. β-actin was used as a loading control.

Figure 5: Gamma-carboxylation is hyper-activated in islets from diabetic mouse models. (A-D) Analysis of *Ins2*$^{+/Akita}$ mice. **(A)** Body weight and **(B)** fed blood glucose were measured weekly. **(C)** At 7-weeks of age, islets of WT and *Ins2*$^{+/Akita}$ mice were harvested, and gene expression analyzed by qPCR (n=4-5). **(D)** Gamma-carboxylation, GGCX and VKORC1 expression were analysed by western blot using anti-Gla, anti-GGCX, and anti-VKORC1 antibodies. β-actin was used as a loading control. **(E-H)** Analysis of *BKS.Lepr*$^{db/db}$ mice. **(E)** Body weight and **(F)** fed blood glucose were measured weekly. **(G)** At 10-weeks of age, islets of *Lepr*$^{db/+}$ and *Lepr*$^{db/db}$ mice were harvested and gene expression analyzed by qPCR (n=5). **(H)** Gamma-carboxylation, GGCX and VKORC1 expression were analysed by western blot using anti-Gla, anti-GGCX, and anti-VKORC1 antibodies. GAPDH was used as a loading control. **(I-K)** Analysis of *B6-Lep*$^{ob/ob}$ mice. **(I)** Body weight and **(J)** fed blood glucose were measured weekly. **(K)** At 9-weeks of age, islets of *Ler*$^{ob/+}$ and *Lep*$^{ob/ob}$ mice were harvested and γ-carboxylation, GGCX and VKORC1 expression were analysed by western blot using anti-Gla, anti-GGCX, and anti-VKORC1 antibodies. β-actin was used as a loading control. **(L-M)** Islets from C57BL/6J mice were cultured for 3 days in media containing either 5 or 15mM glucose. *Ggcx* and *Vkorc1* expression were analyzed by **(L)** qPCR and **(M)** western blot. **(N)** INS-1 832/3 cells

bioRxiv preprint doi: https://doi.org/10.1101/2022.05.13.491370; this version posted May 13, 2022. The copyright holder for this preprint (which was not certified by peer review) is the author/funder, who has granted bioRxiv a license to display the preprint in perpetuity. It is made available under aCC-BY-NC 4.0 International license.

were cultured for 3 days in media containing 2.5 or 25mM glucose in presence of vitamin K (VK_1; 22µM) or vehicle, and GGCX γ-carboxylation was assessed by anti-Gla immunoprecipitation followed by western blot using anti-GGCX antibodies. **(O-P)** Two-months old Wistar rats were infused during 4 days with saline or glucose and **(O)** average blood glucose for the last 3 days of infusion is shown for each mouse**. (P)** Gene expression was analyzed by qPCR (n=3-4) and data were normalized to *Actb*. **(Q)** Human islets from a non-diabetic cadaveric donor (R288) were cultured in presence of VK_1 (22µM) in media containing either 5 or 15mM glucose for 3 days. Gamma-carboxylation and GGCX expression were analysed by western blot using anti-Gla and anti-GGCX antibodies. β-actin was used as a loading control. Results represent the mean ± SEM; unpaired two-tailed Student's *t* test; ***$P < 0.001$; **$P < 0.01$; *$P < 0.05$.

Figure 6: Junctate is a γ-carboxylated protein expressed in β-cells. (A) ASPH and junctate γ-carboxylation was assessed in *Vkorc1*$^{+/-}$*;APOE-c1l1*^{73} and *Vkorc1*$^{-/-}$*;APOE-c1l1*^{73} mouse islets by immunoprecipitation with anti-Gla antibody followed by western blot with the anti-A/J-GRD antibody. **(B)** Quantification of expression and γ-carboxylation were measured using arbitrary densitometry units of ASPH and junctate signals. **(C)** ASPH and junctate γ-carboxylation was assessed in wildtype and *Ins2*$^{+/akita}$ mouse islets by immunoprecipitation as in **(A)**. **(D)** Immunofluorescence on pancreas sections from wildtype and *Ins2*$^{+/akita}$ mice using anti-A/J-GRD and anti-insulin antibodies. DAPI was used to stain nuclei. Scale bar: 20µm. **(E)** Average intensity of anti-A/J-GRD staining in insulin positive cells was quantified in wildtype and *Ins2*$^{+/akita}$ islets (n=5-6, and 10 islets per mice were analyzed). Results represent the mean ± SEM; unpaired two-tailed Student's *t* test; *$P < 0.05$. **(F)** Schematic representation of full length junctate, GRD deletions and glutamic acid to aspartic acid residue mutations. **(G-H)** HEK293 cells transfected with the indicated constructs were cultured with VK_1 (22µM) or warfarin (50µM) as specified. FLAG-tagged proteins were immunoprecipitated with anti-FLAG agarose beads followed by western blot with anti-Gla or anti-FLAG antibodies. **(I)** Quantification of γ-carboxylation of junctate mutants was measured using arbitrary densitometry units of anti-Gla over anti-FLAG signals (n=3). Results represent the mean ± SEM; unpaired two-tailed Student's *t* test; #$P < 0.001$ when compared to junctate + VK_1. **(J)** Representative LC-MS/MS spectrum showing a carboxylated residue in the peptide ranging from residue 289 to 316 in purified Junctate-3XFLAG expressed in HEK293 grown in presence of VK_1. **(K)** Schematic representation of junctate depicting the total number of spectrum counts and the total number of carboxylated spectrum

bioRxiv preprint doi: https://doi.org/10.1101/2022.05.13.491370; this version posted May 13, 2022. The copyright holder for this preprint (which was not certified by peer review) is the author/funder, who has granted bioRxiv a license to display the preprint in perpetuity. It is made available under aCC-BY-NC 4.0 International license.

counts detected when junctate is expressed in HEK293 cells in presence of VK_1 or warfarin, or expressed in *E. coli*.

Figure 7: Junctate γ-carboxylation regulates calcium flux in β-cells. (A) 1 µg of junctate-3XFLAG purified from HEK293 cells cultured with VK_1 (carboxylated) or warfarin (uncarboxylated) was stained with Coomassie and γ-carboxylation monitored by western blot using anti-Gla antibodies. Anti-FLAG was used as a loading control. **(B)** Representative calcium overlay assay. Membrane-immobilized carboxylated and non-carboxylated junctate-3XFLAG were incubated with $^{45}Ca^{2+}$ and radioactivity detected using a storage phosphorimager screen. **(C)** Quantification of calcium binding was measured using arbitrary densitometry units (n=3). Results represent the mean ± SEM; two-way ANOVA with Bonferroni's post tests; ***$P < 0.001$. **(D)** *Asph/Junctate*$^{-/-}$ HEK293 cells were transfected with STIM1-Myc, Orai1-HA and junctate-3XFLAG in presence or not of VK_1 as indicated. Expression and γ-carboxylation were monitored by western blot using anti-Myc, anti-HA, anti-FLAG and anti-Gla antibodies. **(E)** Representation of the strategy used to measure and quantify store-operated calcium entry (SOCE) by live-cell imaging. Fluo-4 loaded cells were incubated in calcium-free buffer containing EGTA, ER-calcium store depleted with thapsigargin (1µM) and SOCE activated by the addition of $CaCl_2$ at the indicated times. **(F)** Fluo-4 calcium traces for each condition are represented as the relative intensity (Fluo-4 intensity/F0). **(G-H)** Quantification of **(G)** ER calcium depletion and **(H)** SOCE are represented as ΔF1 and ΔF2 respectively (n=9). Results represent the mean ± SEM; ordinary one-way ANOVA with Bonferroni's multiple comparisons tests; **$P < 0.01$; *** $P < 0.001$. **(I)** Representative confocal immunofluorescence images of *Asph/Junctate*$^{-/-}$ HEK293 treated with thapsigargin (1µM) or vehicle (DMSO) for 15 minutes and labeled with anti-Myc (STIM1) and anti-HA (Orai1) antibodies. DAPI was used to stain nuclei. Scale bar: 20µm. **(J)** Quantification of puncta characterized by STIM1 and Orai1 colocalization (puncta#/$\mu m^2 x10^3$) (n=30). Results represent the mean ± SEM; ordinary one-way ANOVA with Bonferroni's multiple comparisons tests; *** $P < 0.001$. **(K)** ASPH, junctate and GGCX γ-carboxylation were assessed in *Ggcx*^{ff}*; Ins1-Cre* and *Ins1-Cre* mouse islets by immunoprecipitation with anti-Gla antibody followed by western blot with anti-A/J-GRD or anti-GGCX antibodies. **(L)** SOCE was measured by live-cell calcium imaging in semi-dispersed islets from *Ggcx*^{ff}*;Ins1-Cre* and *Ins1-Cre* mice. Calcium traces are represented as relative intensity (Fluo-4/Fura-Red). **(M)** Basal cytosolic calcium level and **(N)** SOCE (ΔF) quantifications are represented (n=7). **(O-Q)** Cytosolic calcium level was measured at 5 and 15mM glucose and with 30mM KCl for the indicated times. **(O)** Calcium traces for each condition are represented as the relative intensity (Fluo-4/Fura-Red). **(P)** Basal cytosolic calcium level and **(Q)** glucose-stimulated calcium entry (ΔF)

bioRxiv preprint doi: https://doi.org/10.1101/2022.05.13.491370; this version posted May 13, 2022. The copyright holder for this preprint (which was not certified by peer review) is the author/funder, who has granted bioRxiv a license to display the preprint in perpetuity. It is made available under aCC-BY-NC 4.0 International license.

quantifications are represented (n=8). Results represent the mean ± SEM; unpaired two-tailed Student's *t* test; ***P* < 0.01; *** P < 0.001. **(R)** Model of the role of γ-carboxylation in β-cells. In normal conditions, γ-carboxylated junctate (Gla) modulates SOCE by regulating STIM1 and Orai1 puncta formation to maintain calcium homeostasis in β-cells. In absence of GGCX, uncarboxylated junctate (Glu) is less efficient at refraining SOCE, which increases cytosolic calcium levels in β-cells. The combination of excess of nutrient (short HFD) and the rise of cytosolic calcium could lead to elevated fasting serum insulin levels. In diabetic mouse islets, characterized by chronic ER stress and elevated cytosolic calcium, GGCX expression and junctate γ-carboxylation are increased, likely as a compensatory mechanism to reduce cytosolic calcium levels and restore β-cell function.

bioRxiv preprint doi: https://doi.org/10.1101/2022.05.13.491370; this version posted May 13, 2022. The copyright holder for this preprint (which was not certified by peer review) is the author/funder, who has granted bioRxiv a license to display the preprint in perpetuity. It is made available under aCC-BY-NC 4.0 International license.

METHODS

Experimental Model and Subject Details

Mice

Ggcx^{ff} mice were generated in our laboratory as described before (Ferron et al., 2015), and maintained on a C57BL/6J genetic background. These mice were bred to the *Pdx1-Cre* (B6.FVB-*Tg(Pdx1-cre)*^{6Tuv}/Nci; National Cancer Institute; Stock 01XL5) (Hingorani et al., 2003) or the *Ins1-Cre* (B6(Cg)-*Ins1*$^{tm1.1(cre)Thor}$/J; The Jackson Laboratory; Stock 026801) (Thorens et al., 2015) lines to generate *Ggcx*^{ff}*; Pdx1-Cre* and *Ggcx*^{ff}*; Ins1-Cre* mice. β-cells were labeled with the tdTomato reporter gene by breeding the B6.Cg-*Gt(ROSA)26Sor*$^{tm14(CAG-tdTomato)Hze}$/J (Jackson Laboratory; stock 007914) mice to the *Ins1-Cre* strain. *Vkorc1*^{ff} and *Vkorc1l1*^{ff} mice were generated in our laboratory as described before (Ferron et al., 2015), bred to the *Pdx1-Cre* line to generate *Vkorc1*^{ff}*; Vkorc1l1*^{ff}*; Pdx1-Cre* mice and maintained on a C57BL/6J background. Other mouse strains used in this study include BKS.Cg-*Dock7*^{m} +/+ *Lepr*^{db}/J (Jackson Laboratory; Stock 000642), B6.Cg-*Lep*^{ob}/J (Jackson Laboratory; Stock 000632), C57BL/6-*Ins2*^{Akita}/J (Jackson Laboratory; Stock 003548) and *Vkorc1*$^{-/-}$*; APOE-c1l1*^{73} (Lacombe et al., 2018). Male mice were used in all experiments and littermates with the appropriate genotypes always used as controls. Animals were housed at the IRCM in a pathogen-free facility on a 12h light/dark cycle and fed a normal chow diet (Teklad global 19% protein extruded rodent diet; 2919; Envigo), unless otherwise specified. All animal use complied with the guideline of the Canadian Committee for Animal Protection and was approved by IRCM institutional animal care committee.

Human islets

Cadaveric human islets were obtained from the IsletCore at the Alberta Diabetes Institute from the University of Alberta (Edmonton, Alberta, Canada). Upon arrival, islets were handpicked and processed for experiments. When needed, human islets were cultured in DMEM (5mM glucose, 10% FBS, penicillin/streptomycin) in an incubator at 37ºC, 5% CO_2. Detailed protocols for islet isolation and static glucose-stimulated insulin secretion are available in the protocols.io repository (Lyon et al., 2019). Donor characteristics are described in Table S1. The IRCM Ethics committee approved human islets use.

Cell lines

Rat insulinoma cell line INS-1 832/3 (Millipore Sigma) was cultured in RPMI-1640 supplemented with 2mM L-Glutamine, 1mM sodium pyruvate, 10mM HEPES, 0.05 mM β-mercaptoethanol, 10% fetal

bioRxiv preprint doi: https://doi.org/10.1101/2022.05.13.491370; this version posted May 13, 2022. The copyright holder for this preprint (which was not certified by peer review) is the author/funder, who has granted bioRxiv a license to display the preprint in perpetuity. It is made available under aCC-BY-NC 4.0 International license.

bovine serum (FBS) and penicillin/streptomycin as previously described (Ronnebaum et al., 2008). HEK293 cells (ATCC) were cultured in EMEM supplemented with heat-inactivated FBS and penicillin/streptomycin. Cells were cultured at 37ºC with 5% CO_2.

Generation of *Asph/Junctate*$^{-/-}$ HEK 293 cells by CRISPR-Cas9

HEK 293 cells (ATCC) were transfected with single guide RNA (sgRNA; Thermo Fisher) and recombinant *Streptococcus pyogenes* Cas9 protein (SpCas9; Synthego) using Lipofectamine CRISPRMAX Cas9 Transfection reagent (CMAX00001; Thermo Fisher) according to the manufacturer protocol. We selected a sgRNA (Assay ID: CRISPR671774_SGM; Target DNA Sequence: GGACATCTGTAGCTGTCGTT) matching a sequence in the exon 2 of the gene *ASPH* which is shared by all the isoforms encoded by this gene, including ASPH and junctate proteins. Forty-eight hours after the transfection, cells were diluted and seeded in 96-wells plates to establish clonal lines. A total of ninety-six clones were screened by standard Sanger DNA sequencing of the targeted region and the sequence analyzed using the Inference of CRISPR Edits (ICE) Analysis tools of Synthego (https://ice.synthego.com/). Two clones with frameshift-inducing indel on all alleles of *ASPH* were selected and loss of expression of ASPH and junctate confirmed by western blot experiment and by quantitative PCR (Fig. S7A-B).

Rats and infusion

Two-month-old male Wistar rats (Charles River, Saint-Constant, QC, Canada) underwent catheterization of the jugular vein for infusions and the carotid artery for sampling as described (Hagman et al., 2008). Animals were randomized into two groups receiving 0.9% saline (Baxter, Mississauga, ON, Canada; SAL) or 70% dextrose (McKesson, Montreal, QC, Canada; GLU) as described (Moulle et al., 2017). The glucose infusion rate was adjusted to maintain plasma glucose between 13.9 and 19.4 mmol/l throughout the 72h infusion. All procedures were approved by the Institutional Committee for the Protection of Animals at the Centre Hospitalier de l'Université de Montréal.

bioRxiv preprint doi: https://doi.org/10.1101/2022.05.13.491370; this version posted May 13, 2022. The copyright holder for this preprint (which was not certified by peer review) is the author/funder, who has granted bioRxiv a license to display the preprint in perpetuity. It is made available under aCC-BY-NC 4.0 International license.

Method Details

Mouse islet isolation, cell sorting and culture

Mice were anesthetized by intraperitoneal (i.p.) injection of a drug mixture of ketamine hydrochloride and xylazine, sacrificed via cervical dislocation and exsanguinated. The pancreatic duct was perfused with Liberase TL (Roche Applied Science) in Hank's balanced salt solution (HBSS) containing Ca^{2+}/Mg^{2+} and the inflated pancreas was excised and incubated at 37°C for 30 minutes with firm agitation at the 15-minute mark. The digested pancreas was then washed 4 times by decantation with HBSS containing 0.1% BSA and 20mM HEPES pH 7.4, and islets were isolated using Histopaque-1077 density gradient separation (Millipore Sigma). Islets were then transferred to culture media (RPMI, 10% FBS, penicillin/streptomycin) and handpicked under a stereomicroscope (SteREO Discovery.V12; Zeiss).

Islets from *Ins1*$^{Cre/+}$;*Rosa26*$^{CAG\text{-}lox\text{-}stop\text{-}lox\text{-}tdTomato}$ mice were dissociated by incubating at 37ºC for 2 minutes using 0.05% Trypsin-ETDA and pipetting. β-cells (Tom+) and the other islet endocrine cells (Tom-) were sorted out based on tdTomato expression using the FACSAria III cell sorter (Becton Dickinson). Dead cells were excluded based on DAPI staining and only singlets were sorted.

INS-1 832/3 and islet treatments

To test the presence of γ-carboxylation, INS-1 832/3 cells and human islets were cultured in their respective culture media containing either VK_1 (22µM; V3501; MilliporeSigma), warfarin (50µM; SC-204941; Santa Cruz Biotechnology) or vehicle during 3 days before analysis. To assess if γ-carboxylation is regulated by glucose, INS-1 832/3 cells, C57BL/6J islets and human islets were cultured in their respective media with different concentrations of glucose during the 3-day-period in presence of VK_1. To test the protective effect of VK_1, INS-1 832/3 cells were cultured during 2 days with VK_1 or vehicle before 24-hour treatment with media containing 25mM glucose and thapsigargin (10-40nM; 1138; Tocris).

Metabolic analysis

For mice fed a regular chow diet, metabolic analysis was performed as follows. For glucose tolerance tests (GTT), mice were fasted for 16 hours, and blood glucose levels were measured after fasting and at 15, 30, 60 and 120 minutes following i.p. injection of glucose (2g/kg of BW). In vivo glucose-stimulated insulin secretion (GSIS) was measured after 16 hours of fasting. Tail vein blood was

bioRxiv preprint doi: https://doi.org/10.1101/2022.05.13.491370; this version posted May 13, 2022. The copyright holder for this preprint (which was not certified by peer review) is the author/funder, who has granted bioRxiv a license to display the preprint in perpetuity. It is made available under aCC-BY-NC 4.0 International license.

collected after fasting and at 15 and 30 minutes post-injection (i.p.) with glucose (3g/kg of BW). Serum insulin was measured using ELISA (Insulin ELISA mouse; Mercodia). Insulin tolerance test (ITT) was performed after 4 hours of fasting following i.p. injection of insulin (1U/kg; Humulin R, Lilly) and blood glucose was measured after fasting and 30, 60, 90 and 120 minutes post-injection.

For short high fat diet feeding, 10-weeks old mice were fed either a lard-based diet (60% kcal from fat; TD.06414; Envigo) or an ingredient matched control diet (10% kcal from fat; TD.08806; Envigo) for 7 days, after which body weight, random fed blood glucose and metabolic tests were performed. For GSIS tests, tail vein blood glucose was collected after 5 hours of fasting and at 15 and 30 minutes post-injection (i.p.) with glucose (2g/kg). Serum insulin was measured using ELISA and data represented in absolute value or as stimulation index (insulin concentration at 15 or 30 minutes / insulin concentration at fasting). For GTTs, tail vein blood glucose was collected after 5 hours of fasting and at 15, 30, 60 and 120 minutes post-injection (i.p.) with glucose (1.5g/kg).

O_2 consumption, CO_2 release, food intake and physical activity were analyzed using an 8-chamber Promethion Continuous Metabolic System (Sable Systems International) as before (Ferron et al., 2015). Briefly, after a 48-hour acclimation period, data were collected for 96 hours. Energy expenditure (kcal/hour) was calculated by indirect calorimetry using the following formula: 60 x (0.003941 x VO_2 (ml/min) + 0.001106 x VCO_2 (ml/min)). Physical activity was measured as beam breaks for the x-, y- and z-axis using infrared beams connected to the system.

Pancreas immunohistochemistry, immunofluorescence and insulin content

Pancreases were weighed and fixed in 10% formalin for 24 hours at room temperature, embedded in paraffin and sectioned at 5µm. For immunohistochemistry and immunofluorescence experiments, rehydration was followed by an antigen retrieval step (sub-boiling for 10 minutes in 10mM sodium citrate pH 6.0).

For β-cell mass quantifications, insulin was detected using rabbit anti-insulin antibodies (1:200, sc-9168; Santa Cruz Biotechnology), Vectastain Elite ABC-peroxidase kit (Vector Laboratories; PK-6101) and NovaRED Substrate Kit (Vector Laboratories; SK-4800) following manufacturer's instructions. Pancreas tissue was counterstained using Mayer's hematoxylin and histomorphometric analyses were

bioRxiv preprint doi: https://doi.org/10.1101/2022.05.13.491370; this version posted May 13, 2022. The copyright holder for this preprint (which was not certified by peer review) is the author/funder, who has granted bioRxiv a license to display the preprint in perpetuity. It is made available under aCC-BY-NC 4.0 International license.

performed using the OsteoMeasure Analysis System (Osteometrics). β-cell mass was calculated as follows: β-cell area (%) x pancreas weight (mg) / 100.

For immunofluorescence, blocking was performed in PBS containing 5% normal donkey serum and 0.3% Triton for 1 hour at room temperature. Sections were then incubated with antibodies diluted in PBS, 1% BSA and 0.1% Triton, first with goat anti-insulin antibodies (sc-7839; Santa Cruz Biotechnology) and rabbit anti-A/J-GRD antibodies (generated in our laboratory, see below) over-night at 4ºC, and second with Alexa-Fluor 594- conjugated donkey anti-goat (705-585-147; Jackson Immunoresearch Laboratories) and Alexa-Fluor 488-conjugated donkey anti-rabbit (711-545-152; Jackson Immunoresearch Laboratories) antibodies for 1 hour at room temperature. Nuclei were stained with DAPI. Volocity 6.0 quantitation module was used to threshold for and select Insulin$^+$ cells then determine the intensity of the A/J-GRD signal in Insulin$^+$ areas.

For apoptosis detection, the Click-iT Plus TUNEL Assay kit (C10617; Invitrogen) was used following manufacturer's instructions except the proteinase K treatment was replaced by a 10-minute incubation in citrate buffer. Goat anti-insulin antibodies (sc-7839; Santa Cruz Biotechnology) and Alexa-Fluor 594- conjugated donkey anti-goat antibodies (705-585-147; Jackson Immunoresearch Laboratories) were used as described above. Nuclei were stained with DAPI. Insulin$^+$ TUNEL$^+$ cells were detected using the automated DM5500B fluorescence microscope (Leica) with a Retiga EXi (QImaging) and 40X objective. Volocity 6.0 quantitation module was used to threshold for and count Insulin$^+$ cells with TUNEL$^+$ nuclei.

For pancreatic insulin content measures, each pancreas was weighed and homogenized in an acid-ethanol buffer (1.5% HCl; 70% EtOH) after overnight fasting and 2 hours of refeeding. Samples were neutralized using 1M Tris-HCl pH 7.5 (1:1) and insulin measured by ELISA (Mercodia). Insulin content was normalized to the pancreas weight.

RNA isolation and qPCR

For mouse and human islets gene expression analysis, 20-40 handpicked islets per sample were lyzed in guanidium thiocyanate lysis solution, and tRNA (20ug) was added before total RNA was isolated as described (Chomczynski and Sacchi, 2006). Samples were then treated with DNaseI (18068015; Invitrogen), and mRNA reversed transcribed using M-MLV reverse transcriptase (28025013;

bioRxiv preprint doi: https://doi.org/10.1101/2022.05.13.491370; this version posted May 13, 2022. The copyright holder for this preprint (which was not certified by peer review) is the author/funder, who has granted bioRxiv a license to display the preprint in perpetuity. It is made available under aCC-BY-NC 4.0 International license.

Invitrogen) and random hexamers and oligo dT primers. Relative gene expression was quantified using PowerUp SYBR Green Master Mix (A25741; Applied Biosystems) and ViiA7 Real-Time PCR System (Applied Biosystems).

DNA constructs and transfections

Mouse ASPH-3XFLAG and Junctate-3XFLAG plasmids were generated by PCR amplification using pENTR223.1-ASPH (Clone ID: BC166658; Transomic Technologies) as a template and cloning in the HindIII and BamHI restriction sites of the p3XFLAG-CMV-14 expression vector (MilliporeSigma). Human Junctate-3XFLAG was cloned using the same strategy except that MO70-hJunctate plasmid (79596; Addgene) was used as a template. ASPH-3XFLAG and Junctate-3XFLAG deletion mutants were generated by PCR using Q5 High Fidelity DNA polymerase (M0491; NEB) and primers extending in opposite directions and flanking the region to be deleted. Junctate DNA fragments containing glutamic acid to aspartic acid point mutations were synthesized (Genscript) and cloned into Junctate-3XFLAG plasmid via an internal StuI site and the 3' BamHI site. Mouse Orai-HA was generated in two steps. First, the 3' region of Orai1 was cloned from pCMV-SPORT6-Orai1 (BC023149; Transomic Technologies) in the EcoRI and XbaI restriction sites of a pcDNA3.1-Myc-His B expression vector with an HA tag. The missing 5' base pairs of Orai1 were cloned from mouse osteoblast cDNA in the EcoRI and Orai1 internal ApaI restriction sites. Mouse pcDNA3.1-Stim1-Myc plasmid was obtained from Addgene (17732).

HEK293 cells were transfected with "tagless" pCDNA3.1-GGCX and pCDNA3.1-VKORC1 to ensure maximal γ-carboxylation, and with the indicated plasmids using Lipofectamine 2000 transfection reagent (11668019; Invitrogen) following manufacturer's instructions. Six hours post-transfection, media was changed and VK_1 (22μM) or warfarin (50μM) was added when specified. Generation of a clonal cell line stably expressing junctate-3XFLAG was generated via transfection of HEK293 cells with the pJunctate-3XFLAG-CMV-14 plasmid previously linearized by digestion with ScaI. Cells with integration of the plasmid were selected using G418 antibiotics and isolated colonies were expanded. Junctate expression was assessed by western blot using anti-FLAG antibodies and immunofluorescence confirming clonality.

bioRxiv preprint doi: https://doi.org/10.1101/2022.05.13.491370; this version posted May 13, 2022. The copyright holder for this preprint (which was not certified by peer review) is the author/funder, who has granted bioRxiv a license to display the preprint in perpetuity. It is made available under aCC-BY-NC 4.0 International license.

Calcium overlay

HEK293 cells stably expressing mouse Junctate-3XFLAG, and transfected with GGCX and VKORC1, were cultured in the presence of either VK_1 (22μM) or warfarin (10μM). Purified carboxylated and uncarboxylated junctate-3XFLAG proteins were resolved by SDS-PAGE, transferred to a nylon membrane and cross-linked with 0.5% glutaraldehyde. The membrane was quenched with 50mM glycine and washed 3 times with binding buffer containing 60mM KCl, 5mM $MgCl_2$, 10mM imidazole-HCl, pH 6.8, and then incubated with radiolabelled binding buffer containing 8.8μM $^{45}CaCl_2$ (PerkinElmer) for 1 hour, washed with distilled H_2O and dried. Radioactivity was captured by a storage phosphor screen and detected by a laser scanner imaging system (Typhoon FLA 9500; Cytiva).

Generation of rabbit polyclonal anti-Asph/Junctate-GRD antibodies

Rabbit junctate ER luminal domain anti-serum was generated by immunizing rabbits with a 6XHIS tagged protein containing amino acid 85-310 of junctate (MediMabs). Antibodies specific to the glutamic acid rich domain (GRD) were affinity purified using a GST-tagged protein corresponding to the GRD. The specificity of the antibody towards the GRD of junctate and ASPH was tested by western blot.

Immunoprecipitation and western blot

Cells or tissues were homogenized in lysis buffer containing 20mM Tris-HCl (pH 7.5), 150mM NaCl, 1mM EDTA (pH 8.0), 1mM EGTA, 2.5mM NaPyrophosphate, 1mM β-glycerophosphate, 10mM NaF, 1% Triton, 1mM phenylmethylsulfonyl fluoride (PMSF) and protease inhibitors (4693132001; Roche Diagnostics). For anti-Gla immunoprecipitation, 200μg of protein extracts were incubated with 10μg of rabbit anti-Gla antibodies overnight with rotation at 4ºC followed by 3 hours incubation with Protein A-Agarose beads (11719408001; Roche Diagnostics) and washed 4 times with lysis buffer. Immunoprecipitated proteins were heated at 70ºC in Laemmli buffer for 10 minutes before resolving on a 7.5% polyacrylamide Tris-Glycine gels. Proteins were detected using standard western blot procedures with rabbit anti-GGCX (16209-1-AP; ProteinTech) or rabbit anti-A/J antibodies generated in our laboratory (see above). For anti-A/J-GRD IP, the same procedure was followed. FLAG-tagged proteins were immunoprecipitated from 100μg of protein extracts using anti-FLAG agarose beads (A2220; MilliporeSigma) incubated for 2 hours with rotation at 4ºC. Densitometry analyses were performed with the Image Lab software (version 5.0; Bio-Rad Laboratories).

bioRxiv preprint doi: https://doi.org/10.1101/2022.05.13.491370; this version posted May 13, 2022. The copyright holder for this preprint (which was not certified by peer review) is the author/funder, who has granted bioRxiv a license to display the preprint in perpetuity. It is made available under aCC-BY-NC 4.0 International license.

Other antibodies used for western blot in this study include rabbit anti-VKORC1 generated in our laboratory and previously reported (Ferron et al., 2015), rabbit anti-cleaved Caspase-3 (9661; Cell Signaling), rabbit anti-phospho(Ser139)-Histone H2A.X (9718; Cell Signaling), mouse anti-β-Actin (A1978; MilliporeSigma), rabbit anti-GAPDH (5174; Cell Signaling), mouse anti-Myc (2276; Cell Signaling), rabbit anti-HA (C29F4; Cell Signaling), mouse anti-FLAG (F1804; MilliporeSigma) and rabbit anti-FLAG (14793; Cell Signaling). To detect VKORC1, cleaved Caspase-3 and p(Ser139)-Histone H2A.X, proteins were resolved on 10% polyacrylamide Tris-Tricine gels.

Calcium live-cell imaging

Asph/Junctate$^{-/-}$ HEK 293 cells were transfected with GGCX, VKORC1, junctate-3XFLAG, STIM1-Myc and Orai1-HA as indicated and the next day cells were plated on poly-L-lysine (P1274; MilliporeSigma) coated glass coverslips (18mm diameter, #1.5 thickness; 72290-08; Electron Microscopy Sciences). Coverslips were coated with 0.1mg/mL poly-L lysine in sterile ddH_2O at room temperature for 1 hour, before being washed three times with sterile ddH_2O and left to dry for 2 hours. HEK293 cells were loaded with 2μM Fluo-4 AM (F14201; Invitrogen) in Ringer's solution (120mM NaCl, 5mM KCl, 0.8mM $MgSO_4$, 2mM $CaCl_2$, 10mM Glucose, 20mM HEPES, pH 7.4) containing 0.02% pluronic F-127 (P6866; Invitrogen) at 37°C for 30 minutes. Cells were then washed twice with Ringer's solution and incubated for an additional 30 minutes at 37°C to allow complete de-esterification of intracellular AM esters. Calcium imaging was performed in Ca^{2+} free Ringer's solution containing 1mM EGTA. Baseline fluorescence (F0) was measured for 120 seconds before ER calcium stores were depleted by adding thapsigargin (final 1μM) and SOCE was triggered by adding $CaCl_2$ (final [Ca^{2+}] 2mM) 420 seconds after starting recording. Imaging of HEK293 cells was performed at 37°C.

In other experiments, isolated mouse islets were semi-dispersed by digestion with 0.025% Trypsin-ETDA for 1 minute followed by up and down pipetting then transferred to islet culture media containing 22μM VK_1. Semi-dispersed islets enclosed in 200 μL droplets (corresponding to approximately 100 islets) were plated on glass coverslips and allowed to attach for 30 minutes at 37°C, before adding 1mL of islet media for over-night recovery. Islet cells were then loaded with 5μM Fluo-4 AM and 2.5μM Fura-Red AM (F3021; Invitrogen) in HBSS (114mM NaCl, 1.2mM KH_2PO_4, 4.7mM KCl, 1.16mM $MgSO_4$, 25.5mM $NaHCO_3$, 2.5mM $CaCl_2$, 5mM Glucose, 20mM HEPES, 0.2% fatty acid free bovine serum albumin (BSA)) for 30 minutes at room temperature. Baseline fluorescence (F0)

bioRxiv preprint doi: https://doi.org/10.1101/2022.05.13.491370; this version posted May 13, 2022. The copyright holder for this preprint (which was not certified by peer review) is the author/funder, who has granted bioRxiv a license to display the preprint in perpetuity. It is made available under aCC-BY-NC 4.0 International license.

was measured for 90 seconds and response to 15mM glucose was recorded during 90-1700 seconds before KCl concentration was raised to 30mM. SOCE in islet cells was measured as described above but in HBSS containing 200µM diazoxide (D9035; MilliporeSigma) and 10µM verapamil (V4629; Millipore Sigma) for the duration of imaging. Imaging for islets was performed at 32°C and 5% CO_2 enrichment.

Imaging was performed on a confocal rotary disk inverted microscope from Zeiss equipped with a Yokogawa CSU-1 module. The microscope stage contained a conduction heater and was enclosed by an incubator to maintain cells at the desired temperature and CO_2 percentage. Fluo-4 was excited with a 488nm laser and emission was recorded at 509nm (ZEN blue software). Laser power was set to 5%, exposure to 250ms, and EM gain to 500. One image was taken every 5 seconds. Fura-Red was excited with a 488nm laser and emission was recorded at 660nm (ZEN blue software). Laser power was set to 20%, exposure to 500ms, and EM gain to 750. One image was taken every 5 seconds.

Quantification was performed using Fiji (Schindelin et al., 2012). Timelapses were 16-bit greyscale image stacks saved as Carl Zeiss Image data format files. Individual cells or islet clusters were selected as freehand selections to generate regions of interest (ROI). The mean gray value of each ROI was then measured for each image (1 per 5 seconds). Cells that did not stay attached during the entire protocol were excluded from analysis. Measurements at baseline were averaged and used to normalize all subsequent time points (F/F0 = ΔF). When Fluo-4 and Fura-Red were used simultaneously, Fluo-4 fluorescence intensity was divided by Fura-red. All ROI in a given field of view were averaged together for each replicate.

STIM1-Orai1 puncta and STIM1-junctate colocalization

Asph/Junctate$^{-/-}$ HEK293 cells were transfected and plated on poly-L-lysine coated glass coverslip as detailed in the calcium live imaging section. Two days later, cells were equilibrated in Ringer's solution for 45 minutes and treated with 1µM thapsigargin for 15 minutes in Ca^{2+} free Ringer's solution containing 1mM EGTA. Cells were then fixed in 4% paraformaldehyde for 15 minutes at room temperature and washed 3 times with PBS. Cells were stained using anti-FLAG (Cell Signalling; 14793S), anti-Myc (Cell Signalling; 2276) and anti-HA (Cell Signalling; 3724) antibodies as detailed in the immunofluorescence section.

bioRxiv preprint doi: https://doi.org/10.1101/2022.05.13.491370; this version posted May 13, 2022. The copyright holder for this preprint (which was not certified by peer review) is the author/funder, who has granted bioRxiv a license to display the preprint in perpetuity. It is made available under aCC-BY-NC 4.0 International license.

Quantification of puncta was performed using the Volocity 6.0 quantitation module. Puncta were determined via adjusting an intensity threshold and including only objects between 0.1-1.0μm^2 in surface area. Colocalization of junctate-FLAG and STIM1-Myc was also determined via the Volocity 6.0 quantitation module which generated an overlap coefficient and Pearson's coefficient for the two signals within the bounds of manually selected cells. Saturated pixels were excluded from quantification.

RNA-sequencing

Total RNA from islets was extracted using the RNeasy Plus Mini Kit (74134; Qiagen) following manufacturer's instructions (n=4 for each genotype). RNA integrity was evaluated using the 2100 Bioanalyzer system (Agilent) and samples with RIN >7.5 were used. From 1µg of total RNA, poly(A)+ transcripts were enriched using the NEBNext Poly(A) Magnetic isolation module (E7490; NEB) and libraries prepared using the KAPA stranded RNA-seq library preparation kit (KR0934; Roche Diagnostics) and the TruSeq DNA library Prep LT kit (Illumina) according to the manufacturer's procedures. Clustering of the equimolar libraries in the flowcell was performed using the HiSeq PE cluster kit v4 cBot (PE-401-4001; Illumina) and the cBot cluster generation system (Illumina). Sequencing was performed at the Génome Québec Innovation Center using the Illumina HiSeq 2500 system (average of 56 million paired-end reads (PE50) per sample). The quality of the raw reads was assessed with FASTQC v0.11.8. After examining the quality of the raw reads, no trimming was deemed necessary. The reads were aligned to the GRCm38 genome with STAR v2.7.6a with more than 87% of reads uniquely mapped. Raw counts were computed using FeatureCounts v1.6.0 based on Ensembl mouse reference genome v101. Differential expression was performed using the DESeq2 R package and 319 differentially expressed genes (DEGs) were obtained using p-adjusted ≤ 0.05. Gene set enrichment and gene network analyses were performed using StringDB (https://string-db.org/) interrogating Biological Process (Gene Ontology), KEGG Pathways and Annotated Keywords (UniProt). Enrichment was considered significant if the false discovery rate was <0.05 and only networks of 800 or fewer genes were considered for the analysis. Previously published transcriptomic analysis of islets from pre-diabetic (5-weeks old C57BL/6 mice fed a HFD for 8 weeks) or diabetic (8-weeks old *Lepr*$^{db/db}$ and 7-weeks old *Ire1α*^{ff}*; Ins2-Cre*$^{ERT/+}$) mouse models (Lee et al., 2020; Motterle et al., 2017; Wang et al., 2012), were downloaded directly from the publications or from GEO (https://www.ncbi.nlm.nih.gov/geo/). Up-regulated and down-regulated genes for each model were

bioRxiv preprint doi: https://doi.org/10.1101/2022.05.13.491370; this version posted May 13, 2022. The copyright holder for this preprint (which was not certified by peer review) is the author/funder, who has granted bioRxiv a license to display the preprint in perpetuity. It is made available under aCC-BY-NC 4.0 International license.

selected using different p-adjusted values to limit the variability in the total number of genes included in each list: p<0.05 for *Lepr*$^{db/db}$, p<0.01 for HFD and p<0.001 for *Ire1α*^{ff}*; Ins2-Cre*$^{ERT/+}$. Overlap between the various transcriptomes was next determined using jvenn (http://jvenn.toulouse.inra.fr/app/example.html). The statistical significance between each pair of comparisons was computed using an online tool (http://nemates.org/MA/progs/overlap_stats.html). RNA-seq data have been deposited at GEO and are publicly available as of the date of publication. Accession number is GSE199319.

Identification of carboxylated proteins by LC-MS/MS

Livers from 5-day old WT and *Vkorc1*$^{-/-}$ mice were homogenized in lysis buffer and carboxylated proteins immunoprecipitated as described above followed by three washes with 50mM ammonium bicarbonate. Immunoprecipitated proteins were then digested on-bead with trypsin at 37ºC for 18 hours using 0.25ug of Sequencing grade trypsin (Promega). The samples were then reduced with 9 mM dithiothreitol at 37ºC for 30 minutes and, after cooling for 10 minutes, alkylated with 17 mM iodoacetamide at room temperature for 20 minutes in the dark. The supernatants were acidified with trifluoroacetic acid and cleaned from residual detergents and reagents with MCX cartridges (Waters Oasis MCX 96-well Elution Plate) following the manufacturer's instructions. After elution in 10% ammonium hydroxide /90% methanol (v/v), samples were dried with a Speed-vac, reconstituted under agitation for 15 min in 11 µL of 2%ACN-1%FA and 2.4% of each sample was loaded into a 75 µm i.d. × 150 mm Self-Pack C18 column installed in the Easy-nLC II system (Proxeon Biosystems). The buffers used for chromatography were 0.2% formic acid (buffer A) and 90% acetonitrile/0.2% formic acid (buffer B). Peptides were eluted with a two slopes gradient at a flowrate of 250 nL/min. Solvent B first increased from 2 to 44% in 100 min and then from 44 to 88% B in 20 min. The HPLC system was coupled to Orbitrap Fusion mass spectrometer (Thermo Scientific) through a Nanospray Flex Ion Source. Nanospray and S-lens voltages were set to 1.3-1.7 kV and 50 V, respectively. Capillary temperature was set to 225 °C. Full scan MS survey spectra (m/z 360-1560) in profile mode were acquired in the Orbitrap with a resolution of 120,000 with a target value at 3e5. The 25 most intense peptide ions were fragmented in the HCD cell and analyzed in the linear ion trap with a target value at 2e4 and a collision energy at 29. Target ions selected for fragmentation were dynamically excluded for 30 sec after 2 MS/MS events.

The peak list files were generated with Proteome Discoverer (version 2.3) using the following parameters: minimum mass set to 500 Da, maximum mass set to 6000 Da, no grouping of MS/MS

bioRxiv preprint doi: https://doi.org/10.1101/2022.05.13.491370; this version posted May 13, 2022. The copyright holder for this preprint (which was not certified by peer review) is the author/funder, who has granted bioRxiv a license to display the preprint in perpetuity. It is made available under aCC-BY-NC 4.0 International license.

spectra, precursor charge set to auto, and minimum number of fragment ions set to 5. Protein database searching was performed with Mascot 2.6 (Matrix Science) against the UniProt Mus Musculus protein database. The mass tolerances for precursor and fragment ions were set to 10 ppm and 0.6 Da, respectively. Trypsin was used as the enzyme allowing for up to 1 missed cleavage. Cysteine carbamidomethylation was specified as a fixed modification, and methionine oxidation, glutamic acid carboxylation and phosphorylation S/T/Y as variable modifications. Data interpretation was performed using Scaffold (version 4.8) using a peptide threshold of 80%, a protein threshold of 95% and one peptide minimum. We considered a protein as being carboxylated when the average exclusive spectrum count in WT samples was at least double of the *Vkorc1*$^{-/-}$ samples. To minimize the potential identification of proteins non-specifically binding the anti-Gla antibodies or the agarose-beads, we excluded proteins with more than 2 exclusive spectrum counts in the *Vkorc1*$^{-/-}$ samples or with a difference of less than 2 between the WT and *Vkorc1*$^{-/-}$ samples. The mass spectrometry proteomics dataset have been deposited to the ProteomeXchange Consortium via the PRIDE partner repository (Perez-Riverol et al., 2022) with the dataset identifier PXD032920 and 10.6019/PXD032920.

Identification of carboxylated residues in Junctate by LC-MS/MS

HEK293 cells stably expressing mouse Junctate-3XFLAG were cultured in the presence of either VK_1 (22µM) or warfarin (10µM) for at least 2 weeks, and carboxylated and uncarboxylated Junctate-3XFLAG were purified with anti-FLAG agarose beads (A2220; MilliporeSigma). On-bead proteins were first diluted in 2M Urea/50mM ammonium bicarbonate, and on-bead chymotrypsin digestion was performed overnight at 37ºC. The supernatants were acidified with trifluoroacetic acid and cleaned from residual detergents and reagents with MCX cartridges (Waters Oasis MCX 96-well Elution Plate) following the manufacturer's instructions. After elution in 10% ammonium hydroxide /90% methanol (v/v), samples were dried with a Speed-vac, reconstituted under agitation for 15 min in 11 µL of 2%ACN-1%FA and loaded into a 75 µm i.d. × 150 mm, Self-Pack C18 column, installed in the Easy-nLC II system (Proxeon Biosystems). Peptides were loaded on-column and eluted with a two-slope gradient at a flow rate of 250 nL/min. Solvent B first increased from 1 to 32% in 86 min and then from 32 to 82% B in 22 min. The HPLC system was coupled to Orbitrap Fusion mass spectrometer (Thermo Scientific) through a Nanospray Flex Ion Source. Nanospray and S-lens voltages were set to 1.3-1.8 kV and 50 V, respectively. Capillary temperature was set to 250 °C. Full scan MS survey spectra (m/z 320-1520) in profile mode were acquired in the Orbitrap with a resolution of 120,000 with a target value at 5e5. The most intense peptide ions were fragmented by ETD, CID and ETciD and analysed in the linear ion trap with a target value at 1e4. The peptide ion fragmentation parameters were as follow: a reaction time of 120 ms, a reagent target of 2.0e5 and a maximum reagent

bioRxiv preprint doi: https://doi.org/10.1101/2022.05.13.491370; this version posted May 13, 2022. The copyright holder for this preprint (which was not certified by peer review) is the author/funder, who has granted bioRxiv a license to display the preprint in perpetuity. It is made available under aCC-BY-NC 4.0 International license.

injection time of 200 ms for ETD, a normalized collision energy of 32% for CID, calibrated charge dependent ETD parameters and normalized supplemental activation at 18% for ETciD. The duty cycle was set to 4 seconds and target ions selected for fragmentation were dynamically excluded for 30 sec after 2 MS/MS scan events. Uncarboxylated bacterially produced His-tagged Junctate was digested in-solution with chymotrypsin in the aforementioned conditions.

The peak list files were generated with Proteome Discoverer (version 2.1 or 2.4) using the following parameters: minimum mass set to 500 Da, maximum mass set to 6000 Da, no grouping of MS/MS spectra, precursor charge set to auto, and the minimum number of fragment ions set to 5. Protein database searching was performed with Mascot 2.6 (Matrix Science) against a user-defined mouse junctate database. The mass tolerances for precursor and fragment ions were set to 10 ppm and 0.6 Da, respectively. A semi-specific search was performed using chymotrypsin as the enzyme allowing for up to 1 missed cleavage. Methionine oxidation and carboxylation of glutamic acid were specified as variable modifications. Data interpretation was performed using Scaffold (version 4.8). The mass spectrometry proteomics dataset have been deposited to the ProteomeXchange Consortium via the PRIDE partner repository (Perez-Riverol et al., 2022) with the dataset identifier PXD032955 and 10.6019/PXD032955.

Statistics

Statistical analyses were performed using GraphPad Prism software (version 9.3.1). Results are given as means ± SEM. For single measurement, unpaired, 2-tailed Student's *t* test was used. Grouped analysis was performed using one-way ANOVA, followed by Bonferroni's multiple comparisons test. For repeated measurements (metabolic tests), two-way ANOVA followed by Bonferroni's post tests were used. Linear correlations were analyzed using Pearson's correlation. In all figures, $*P < 0.05$; $**P < 0.01$; $***P < 0.001$. All experiments were repeated at least 3 times or performed on at least 3 independent animals.

DATA AND CODE AVAILABILITY

RNA-seq data have been deposited at GEO and are publicly available as of the date of publication. Accession number is GSE199319.

bioRxiv preprint doi: https://doi.org/10.1101/2022.05.13.491370; this version posted May 13, 2022. The copyright holder for this preprint (which was not certified by peer review) is the author/funder, who has granted bioRxiv a license to display the preprint in perpetuity. It is made available under aCC-BY-NC 4.0 International license.

The mass spectrometry proteomics dataset "Identification of vitamin K-dependent proteins in mouse liver by LC-MS/MS" have been deposited to the ProteomeXchange Consortium via the PRIDE partner repository (Perez-Riverol et al., 2022) with the dataset identifier PXD032920 and 10.6019/PXD032920.

The mass spectrometry proteomics dataset "Identification of gamma-carboxyglutamic acid residues in mouse junctate by LC-MS/MS" have been deposited to the ProteomeXchange Consortium via the PRIDE partner repository (Perez-Riverol et al., 2022) with the dataset identifier PXD032955 and 10.6019/PXD032955.

bioRxiv preprint doi: https://doi.org/10.1101/2022.05.13.491370; this version posted May 13, 2022. The copyright holder for this preprint (which was not certified by peer review) is the author/funder, who has granted bioRxiv a license to display the preprint in perpetuity. It is made available under aCC-BY-NC 4.0 International license.

SUPPLEMENTAL FIGURE LEGENDS

Figure S1, related to Figure 1: *Ggcx* and *Vkorc1* are expressed in pancreatic endocrine cells. (A-B) *Ggcx* and *Vkorc1* gene expression was analyzed by quantitative PCR in various tissues from wild-type (WT) mice and normalized to *Actb*. **(C-D)** Violin plots representing single cell transcriptome data from mouse pancreatic tissues (https://tabula-muris.ds.czbiohub.org/). **(E-F)** *Ggcx* gene expression was analyzed by quantitative PCR in islets from **(E)** *Ggcx^{ff}; Pdx1-Cre*, **(F)** *Ggcx^{ff}; Ins1-Cre* and their respective *Ggcx^{ff}* controls, and normalized to *Actb* or *Gapdh* (n=4-5; mean ± SEM; unpaired, 2-tailed Student's *t* test; ***$P < 0.001$; **$P < 0.01$).

Figure S2, related to Figure 3: Characterization of the *Ggcx^{ff}; Pdx1-Cre* mouse model. (A-C) Metabolic parameters of 32-weeks old *Ggcx^{ff}; Pdx1-Cre* and *Ggcx^{ff}* male mice (n=10). **(A)** Energy expenditure, O_2 consumption, CO_2 production, **(B)** physical activity (x, y and z axis) and **(C)** food intake during day and night was measured using a continuous metabolic system. **(D)** Pancreas weight from 24- to 28-weeks old male mice was determined in fed condition (n=9-13). **(E)** Body weight of *Ggcx^{ff}; Pdx1-Cre* and *Ggcx^{ff}* male mice fed a chow diet was measured weekly. **(F)** Genomic DNA from various tissues from *Ggcx^{ff}; Pdx1-Cre* mice was extracted and used to amplify *Ggcx* by PCR to detect the floxed and excised allele (Δ). **(G-H)** Histomorphometric analysis on pancreas section following insulin staining and hematoxylin counterstaining from **(G)** *Vkorc1^{ff}; Vkorc1l1^{ff}; Pdx1-Cre* (*c1^{ff}; c1l1^{ff}; Pdx1-Cre*) (n=6-9) and **(H)** *Pdx1-Cre* (n=6) 24-weeks old male mice. **(I)** Pancreas from 24-weeks old *Pdx1-Cre* and WT male mice were homogenized, and insulin content measured by ELISA (n=10). Results represent the mean ± SEM. Two-way ANOVA with Bonferroni's multiple comparisons test was used for repeated measurements and unpaired, two-tailed Student's *t* test was used for simple comparison; *$P < 0.05$.

Figure S3, related to Figure 4: 7 days of high fat feeding induces ER-stress in islets. (A-F) *Ggcx^{ff}* control mice were fed either a control low fat, or a high fat diet for 7 days and gene expression in islets was analyzed by qPCR. Data were normalized to *Hprt* (n=4-5). **(G-H)** *Ggcx^{ff}; Pdx1-Cre* and *Ggcx^{ff}* male mice were fed with a control low-fat diet or HFD for 7 days. **(G)** Body weight and **(H)** glucose tolerance (GTT) were measured. **(I-K)** Metabolic analysis of 12-weeks old *Ggcx^{ff}; Ins1-Cre* and *Ins1-Cre* mice on a regular chow diet. **(I)** GTT, **(J)** fasting glucose and **(K)** fasting insulin were measured. **(L-M)** *Ggcx^{ff}; Ins1-Cre* and *Ggcx^{ff}* male mice were fed a HFD for 7 days. **(L)** Body weight and **(M)** glucose tolerance (GTT) were measured. Results represent the mean ± SEM; two-way ANOVA with

bioRxiv preprint doi: https://doi.org/10.1101/2022.05.13.491370; this version posted May 13, 2022. The copyright holder for this preprint (which was not certified by peer review) is the author/funder, who has granted bioRxiv a license to display the preprint in perpetuity. It is made available under aCC-BY-NC 4.0 International license.

Bonferroni's post test was used for repeated measurements; unpaired, 2-tailed Student's *t* test was used for simple comparison; ***$P < 0.001$; **$P < 0.01$; *$P < 0.05$.

Figure S4, related to Figure 6: Junctate isoform is predominant in pancreatic islets. (A-C) Gene expression analysis of mouse islets using RNA-sequencing. **(A)** Expression level of Gla proteins encoding genes in control mouse islets (expressed as read counts normalized to library size). **(B)** Schematic displays of the *Asph* gene locus and of the major *Asph* isoforms. Sashimi plots beneath schematic show the read counts observed for each isoform with exon spanning read counts denoted atop the arches. **(C)** Median read counts in the final and unique exon encoding ASPH, junctate, and junctin. **(D)** Schematic representation of full length ASPH and junctate with their respective deletion mutants. **(E)** HEK293 cells transfected with the indicated constructs were cultured with VK_1 (22μM) or warfarin (50μM) as specified. ASPH and junctate were detected by western blot using anti-A/J-GRD antibodies and anti-FLAG was used as a loading control. **(F-G)** ASPH and junctate γ-carboxylation was assessed in *Vkorc1*$^{+/+}$ and *Vkorc1*$^{-/-}$ 7-day-old mouse livers by **(F)** immunoprecipitation with anti-Gla antibody followed by western blot with the anti-A/J-GRD antibody and by **(G)** immunoprecipitation with anti-A/J-GRD antibodies followed by western blot with anti-Gla antibodies. **(H)** ASPH and junctate γ-carboxylation was assessed in *Vkorc1*$^{+/-}$*;APOE-c1l1*^{73} and *Vkorc1*$^{-/-}$*;APOE-c1l1*^{73} mouse islets by immunoprecipitation with anti-Gla antibody followed by western blot with the anti-A/J-GRD antibody (longer exposure compared to Fig. 6A). **(I)** HEK293 cells transfected with the indicated constructs were cultured with VK_1 (22μM) or warfarin (50μM) as specified. FLAG-tagged proteins were immunoprecipitated with anti-FLAG agarose beads followed by western blot with anti-Gla antibodies. Western blot with anti-FLAG antibodies was used as a loading control. **(J)** Sequence alignment of GRD from mammalian junctate homologues. Sequences from mouse (*M. musculus*), rat (*R. norvegicus*), human (*H. sapiens*), cat (*F. catus*), horse (*H. caballus*), cattle (*B. taurus*), wild boar (*S. scrofa*) and blue whale (*B. musculus*) are shown. Glutamic acid residues are highlighted in green; single asterisk (*) indicates a fully conserved residue; a colon (:) indicates a strongly conserved residue; and a period (.) indicates moderate or weak conservation. **(K)** HEK293 cells transfected with the indicated constructs were cultured with VK_1 (22μM) or warfarin (50μM) as specified. Carboxylated proteins were immunoprecipitated with anti-Gla antibodies followed by western blot with anti-FLAG antibodies. **(L)** Mouse (m) and human (h) junctate expressed in HEK293 cells cultured with VK_1 or warfarin were immunoprecipitated with anti-FLAG agarose beads followed by western blot with anti-Gla or anti-FLAG antibodies.

bioRxiv preprint doi: https://doi.org/10.1101/2022.05.13.491370; this version posted May 13, 2022. The copyright holder for this preprint (which was not certified by peer review) is the author/funder, who has granted bioRxiv a license to display the preprint in perpetuity. It is made available under aCC-BY-NC 4.0 International license.

Figure S5, related to Figure 7: Junctate γ-carboxylation reduces Stim1 puncta formation. (A-B) Efficient knockdown of ASPH and junctate in HEK293 cells was validated by **(A)** western blot and **(B)** qPCR analysis (n=4). Asterisks indicate non-specific binding. Results represent the mean ± SEM; unpaired two-tailed Student's *t* test; ***$P < 0.001$. **(C)** Quantification of puncta characterized by Orai1 (puncta#/$\mu m^2 x10^3$). **(D)** Quantification of puncta characterized by STIM1 (puncta#/$\mu m^2 x10^3$). **(E)** Representative confocal immunofluorescence images of *Asph/Junctate*$^{-/-}$ HEK293 treated with thapsigargin (1μM) or vehicle (DMSO) for 15 minutes and labeled with anti-Myc (STIM1) and anti-FLAG (Junctate) antibodies. DAPI was used to stain nuclei. Scale bar: 20μm. **(F)** Quantification of overlap coefficient of STIM1-Myc and junctate-3XFLAG signals as calculated by Volocity 6.0 quantitation module (n=30). Results represent the mean ± SEM; non-repeated one-way ANOVA with Bonferroni multiple comparisons tests; *** $P < 0.001$. **(G)** ER calcium depletion quantifications in *Ggcx*^{ff}*; Ins1-Cre* and *Ins1-Cre* islets (ΔF) (n=7).

bioRxiv preprint doi: https://doi.org/10.1101/2022.05.13.491370; this version posted May 13, 2022. The copyright holder for this preprint (which was not certified by peer review) is the author/funder, who has granted bioRxiv a license to display the preprint in perpetuity. It is made available under aCC-BY-NC 4.0 International license.

REFERENCES

Bandyopadhyay, P.K., Garrett, J.E., Shetty, R.P., Keate, T., Walker, C.S., and Olivera, B.M. (2002). gamma -Glutamyl carboxylation: An extracellular posttranslational modification that antedates the divergence of molluscs, arthropods, and chordates. Proc Natl Acad Sci U S A *99*, 1264-1269.

Berkner, K.L., and Pudota, B.N. (1998). Vitamin K-dependent carboxylation of the carboxylase. Proc Natl Acad Sci U S A *95*, 466-471.

Beulens, J.W., van der, A.D., Grobbee, D.E., Sluijs, I., Spijkerman, A.M., and van der Schouw, Y.T. (2010). Dietary phylloquinone and menaquinones intakes and risk of type 2 diabetes. Diabetes Care *33*, 1699-1705.

Brouwers, B., de Faudeur, G., Osipovich, A.B., Goyvaerts, L., Lemaire, K., Boesmans, L., Cauwelier, E.J., Granvik, M., Pruniau, V.P., Van Lommel, L., *et al.* (2014). Impaired islet function in commonly used transgenic mouse lines due to human growth hormone minigene expression. Cell Metab *20*, 979-990.

Chabosseau, P., and Rutter, G.A. (2016). Zinc and diabetes. Archives of biochemistry and biophysics *611*, 79-85.

Chomczynski, P., and Sacchi, N. (2006). The single-step method of RNA isolation by acid guanidinium thiocyanate-phenol-chloroform extraction: twenty-something years on. Nature protocols *1*, 581-585.

Clee, S.M., Yandell, B.S., Schueler, K.M., Rabaglia, M.E., Richards, O.C., Raines, S.M., Kabara, E.A., Klass, D.M., Mui, E.T., Stapleton, D.S., *et al.* (2006). Positional cloning of Sorcs1, a type 2 diabetes quantitative trait locus. Nat Genet *38*, 688-693.

Coleman, D.L., and Hummel, K.P. (1973). The influence of genetic background on the expression of the obese (Ob) gene in the mouse. Diabetologia *9*, 287-293.

Consortium, T.M. (2018). Single-cell transcriptomics of 20 mouse organs creates a Tabula Muris. Nature *562*, 367-372.

DiGruccio, M.R., Mawla, A.M., Donaldson, C.J., Noguchi, G.M., Vaughan, J., Cowing-Zitron, C., van der Meulen, T., and Huising, M.O. (2016). Comprehensive alpha, beta and delta cell transcriptomes reveal that ghrelin selectively activates delta cells and promotes somatostatin release from pancreatic islets. Mol Metab *5*, 449-458.

Dihingia, A., Ozah, D., Ghosh, S., Sarkar, A., Baruah, P.K., Kalita, J., Sil, P.C., and Manna, P. (2018). Vitamin K1 inversely correlates with glycemia and insulin resistance in patients with type 2 diabetes

bioRxiv preprint doi: https://doi.org/10.1101/2022.05.13.491370; this version posted May 13, 2022. The copyright holder for this preprint (which was not certified by peer review) is the author/funder, who has granted bioRxiv a license to display the preprint in perpetuity. It is made available under aCC-BY-NC 4.0 International license.

(T2D) and positively regulates SIRT1/AMPK pathway of glucose metabolism in liver of T2D mice and hepatocytes cultured in high glucose. The Journal of nutritional biochemistry *52*, 103-114.

Ewang-Emukowhate, M., Harrington, D.J., Botha, A., McGowan, B., and Wierzbicki, A.S. (2015). Vitamin K and other markers of micronutrient status in morbidly obese patients before bariatric surgery. Int J Clin Pract *69*, 638-642.

Ferdaoussi, M., Dai, X., Jensen, M.V., Wang, R., Peterson, B.S., Huang, C., Ilkayeva, O., Smith, N., Miller, N., Hajmrle, C., *et al.* (2015). Isocitrate-to-SENP1 signaling amplifies insulin secretion and rescues dysfunctional beta cells. J Clin Invest *125*, 3847-3860.

Feriotto, G., Finotti, A., Volpe, P., Treves, S., Ferrari, S., Angelelli, C., Zorzato, F., and Gambari, R. (2005). Myocyte enhancer factor 2 activates promoter sequences of the human AbetaH-J-J locus, encoding aspartyl-beta-hydroxylase, junctin, and junctate. Mol Cell Biol *25*, 3261-3275.

Ferron, M., Lacombe, J., Germain, A., Oury, F., and Karsenty, G. (2015). GGCX and VKORC1 inhibit osteocalcin endocrine functions. J Cell Biol *208*, 761-776.

Furie, B., Bouchard, B.A., and Furie, B.C. (1999). Vitamin K-dependent biosynthesis of gamma-carboxyglutamic acid. Blood *93*, 1798-1808.

Hagman, D.K., Latour, M.G., Chakrabarti, S.K., Fontes, G., Amyot, J., Tremblay, C., Semache, M., Lausier, J.A., Roskens, V., Mirmira, R.G., *et al.* (2008). Cyclical and alternating infusions of glucose and intralipid in rats inhibit insulin gene expression and Pdx-1 binding in islets. Diabetes *57*, 424-431.

Hallgren, K.W., Zhang, D., Kinter, M., Willard, B., and Berkner, K.L. (2013). Methylation of gamma-carboxylated Glu (Gla) allows detection by liquid chromatography-mass spectrometry and the identification of Gla residues in the gamma-glutamyl carboxylase. Journal of proteome research *12*, 2365-2374.

Haque, J.A., McDonald, M.G., Kulman, J.D., and Rettie, A.E. (2014). A cellular system for quantitation of vitamin K cycle activity: structure-activity effects on vitamin K antagonism by warfarin metabolites. Blood *123*, 582-589.

Hingorani, S.R., Petricoin, E.F., Maitra, A., Rajapakse, V., King, C., Jacobetz, M.A., Ross, S., Conrads, T.P., Veenstra, T.D., Hitt, B.A., *et al.* (2003). Preinvasive and invasive ductal pancreatic cancer and its early detection in the mouse. Cancer cell *4*, 437-450.

Hoffman, D.J., Powell, T.L., Barrett, E.S., and Hardy, D.B. (2021). Developmental origins of metabolic diseases. Physiol Rev *101*, 739-795.

bioRxiv preprint doi: https://doi.org/10.1101/2022.05.13.491370; this version posted May 13, 2022. The copyright holder for this preprint (which was not certified by peer review) is the author/funder, who has granted bioRxiv a license to display the preprint in perpetuity. It is made available under aCC-BY-NC 4.0 International license.

Hudish, L.I., Reusch, J.E., and Sussel, L. (2019). beta Cell dysfunction during progression of metabolic syndrome to type 2 diabetes. J Clin Invest *129*, 4001-4008.

Hummel, K.P., Dickie, M.M., and Coleman, D.L. (1966). Diabetes, a new mutation in the mouse. Science *153*, 1127-1128.

Ibarrola-Jurado, N., Salas-Salvado, J., Martinez-Gonzalez, M.A., and Bullo, M. (2012). Dietary phylloquinone intake and risk of type 2 diabetes in elderly subjects at high risk of cardiovascular disease. Am J Clin Nutr *96*, 1113-1118.

Johnson, J.S., Kono, T., Tong, X., Yamamoto, W.R., Zarain-Herzberg, A., Merrins, M.J., Satin, L.S., Gilon, P., and Evans-Molina, C. (2014). Pancreatic and duodenal homeobox protein 1 (Pdx-1) maintains endoplasmic reticulum calcium levels through transcriptional regulation of sarco-endoplasmic reticulum calcium ATPase 2b (SERCA2b) in the islet beta cell. J Biol Chem *289*, 32798-32810.

Kaidar-Person, O., Person, B., Szomstein, S., and Rosenthal, R.J. (2008). Nutritional deficiencies in morbidly obese patients: a new form of malnutrition? Part A: vitamins. Obesity surgery *18*, 870-876.

Karamzad, N., Faraji, E., Adeli, S., Carson-Chahhoud, K., Azizi, S., and Pourghassem Gargari, B. (2020). Effects of MK-7 Supplementation on Glycemic Status, Anthropometric Indices and Lipid Profile in Patients with Type 2 Diabetes: A Randomized Controlled Trial. Diabetes Metab Syndr Obes *13*, 2239-2249.

Kono, T., Tong, X., Taleb, S., Bone, R.N., Iida, H., Lee, C.C., Sohn, P., Gilon, P., Roe, M.W., and Evans-Molina, C. (2018). Impaired Store-Operated Calcium Entry and STIM1 Loss Lead to Reduced Insulin Secretion and Increased Endoplasmic Reticulum Stress in the Diabetic beta-Cell. Diabetes *67*, 2293-2304.

Kwon, S.J., and Kim, D.H. (2009). Characterization of junctate-SERCA2a interaction in murine cardiomyocyte. Biochem Biophys Res Commun *390*, 1389-1394.

Lacombe, J., and Ferron, M. (2018). VKORC1L1, An Enzyme Mediating the Effect of Vitamin K in Liver and Extrahepatic Tissues. Nutrients *10*, E970.

Lacombe, J., Rishavy, M.A., Berkner, K.L., and Ferron, M. (2018). VKOR paralog VKORC1L1 supports vitamin K-dependent protein carboxylation in vivo. JCI Insight *3*, e96501.

bioRxiv preprint doi: https://doi.org/10.1101/2022.05.13.491370; this version posted May 13, 2022. The copyright holder for this preprint (which was not certified by peer review) is the author/funder, who has granted bioRxiv a license to display the preprint in perpetuity. It is made available under aCC-BY-NC 4.0 International license.

Lee, H., Lee, Y.S., Harenda, Q., Pietrzak, S., Oktay, H.Z., Schreiber, S., Liao, Y., Sonthalia, S., Ciecko, A.E., Chen, Y.G., *et al.* (2020). Beta Cell Dedifferentiation Induced by IRE1alpha Deletion Prevents Type 1 Diabetes. Cell Metab *31*, 822-836 e825.

Lee, N.K., Sowa, H., Hinoi, E., Ferron, M., Ahn, J.D., Confavreux, C., Dacquin, R., Mee, P.J., McKee, M.D., Jung, D.Y., *et al.* (2007). Endocrine regulation of energy metabolism by the skeleton. Cell *130*, 456-469.

Liang, K., Du, W., Lu, J., Li, F., Yang, L., Xue, Y., Hille, B., and Chen, L. (2014). Alterations of the Ca(2)(+) signaling pathway in pancreatic beta-cells isolated from db/db mice. Protein Cell *5*, 783-794.

Lunz, V., Romanin, C., and Frischauf, I. (2019). STIM1 activation of Orai1. Cell calcium *77*, 29-38.

Lyon, J., Spigelman, A.F., MacDonald, P.E., and Manning Fox, J.E. (2019). ADI IsletCore Protocols for the Isolation, Assessment and Cryopreservation of Human Pancreatic Islets of Langerhans for Research Purposes V.1. protocolio.

Mehran, A.E., Templeman, N.M., Brigidi, G.S., Lim, G.E., Chu, K.Y., Hu, X., Botezelli, J.D., Asadi, A., Hoffman, B.G., Kieffer, T.J., *et al.* (2012). Hyperinsulinemia drives diet-induced obesity independently of brain insulin production. Cell Metab *16*, 723-737.

Mittendorfer, B., Patterson, B.W., Smith, G.I., Yoshino, M., and Klein, S. (2022). beta Cell function and plasma insulin clearance in people with obesity and different glycemic status. J Clin Invest *132*.

Motterle, A., Gattesco, S., Peyot, M.L., Esguerra, J.L.S., Gomez-Ruiz, A., Laybutt, D.R., Gilon, P., Burdet, F., Ibberson, M., Eliasson, L., *et al.* (2017). Identification of islet-enriched long non-coding RNAs contributing to beta-cell failure in type 2 diabetes. Mol Metab *6*, 1407-1418.

Moulle, V.S., Vivot, K., Tremblay, C., Zarrouki, B., Ghislain, J., and Poitout, V. (2017). Glucose and fatty acids synergistically and reversibly promote beta cell proliferation in rats. Diabetologia *60*, 879-888.

Murshed, M., Schinke, T., McKee, M.D., and Karsenty, G. (2004). Extracellular matrix mineralization is regulated locally; different roles of two gla-containing proteins. J Cell Biol *165*, 625-630.

Oropeza, D., Jouvet, N., Budry, L., Campbell, J.E., Bouyakdan, K., Lacombe, J., Perron, G., Bergeron, V., Neuman, J.C., Brar, H.K., *et al.* (2015). Phenotypic Characterization of MIP-CreERT1Lphi Mice With Transgene-Driven Islet Expression of Human Growth Hormone. Diabetes *64*, 3798-3807.

bioRxiv preprint doi: https://doi.org/10.1101/2022.05.13.491370; this version posted May 13, 2022. The copyright holder for this preprint (which was not certified by peer review) is the author/funder, who has granted bioRxiv a license to display the preprint in perpetuity. It is made available under aCC-BY-NC 4.0 International license.

Pan, Y., and Jackson, R.T. (2009). Dietary phylloquinone intakes and metabolic syndrome in US young adults. J Am Coll Nutr *28*, 369-379.

Perez-Riverol, Y., Bai, J., Bandla, C., Garcia-Seisdedos, D., Hewapathirana, S., Kamatchinathan, S., Kundu, D.J., Prakash, A., Frericks-Zipper, A., Eisenacher, M., *et al.* (2022). The PRIDE database resources in 2022: a hub for mass spectrometry-based proteomics evidences. Nucleic acids research *50*, D543-D552.

Rahimi Sakak, F., Moslehi, N., Niroomand, M., and Mirmiran, P. (2021). Glycemic control improvement in individuals with type 2 diabetes with vitamin K2 supplementation: a randomized controlled trial. Eur J Nutr *60*, 2495-2506.

Riahi, Y., Israeli, T., Yeroslaviz, R., Chimenez, S., Avrahami, D., Stolovich-Rain, M., Alter, I., Sebag, M., Polin, N., Bernal-Mizrachi, E., *et al.* (2018). Inhibition of mTORC1 by ER stress impairs neonatal beta-cell expansion and predisposes to diabetes in the Akita mouse. eLife *7*.

Ronnebaum, S.M., Jensen, M.V., Hohmeier, H.E., Burgess, S.C., Zhou, Y.P., Qian, S., MacNeil, D., Howard, A., Thornberry, N., Ilkayeva, O., *et al.* (2008). Silencing of cytosolic or mitochondrial isoforms of malic enzyme has no effect on glucose-stimulated insulin secretion from rodent islets. J Biol Chem *283*, 28909-28917.

Sabatini, P.V., Speckmann, T., and Lynn, F.C. (2019). Friend and foe: beta-cell Ca(2+) signaling and the development of diabetes. Mol Metab *21*, 1-12.

Sabourin, J., Le Gal, L., Saurwein, L., Haefliger, J.A., Raddatz, E., and Allagnat, F. (2015). Store-operated Ca2+ Entry Mediated by Orai1 and TRPC1 Participates to Insulin Secretion in Rat beta-Cells. J Biol Chem *290*, 30530-30539.

Schindelin, J., Arganda-Carreras, I., Frise, E., Kaynig, V., Longair, M., Pietzsch, T., Preibisch, S., Rueden, C., Saalfeld, S., Schmid, B., *et al.* (2012). Fiji: an open-source platform for biological-image analysis. Nat Methods *9*, 676-682.

Schmidt, T., Samaras, P., Frejno, M., Gessulat, S., Barnert, M., Kienegger, H., Krcmar, H., Schlegl, J., Ehrlich, H.C., Aiche, S., *et al.* (2018). ProteomicsDB. Nucleic acids research *46*, D1271-D1281.

Sharma, R.B., Landa-Galvan, H.V., and Alonso, L.C. (2021). Living Dangerously: Protective and Harmful ER Stress Responses in Pancreatic beta-Cells. Diabetes *70*, 2431-2443.

bioRxiv preprint doi: https://doi.org/10.1101/2022.05.13.491370; this version posted May 13, 2022. The copyright holder for this preprint (which was not certified by peer review) is the author/funder, who has granted bioRxiv a license to display the preprint in perpetuity. It is made available under aCC-BY-NC 4.0 International license.

Sharma, R.B., O'Donnell, A.C., Stamateris, R.E., Ha, B., McCloskey, K.M., Reynolds, P.R., Arvan, P., and Alonso, L.C. (2015). Insulin demand regulates beta cell number via the unfolded protein response. J Clin Invest *125*, 3831-3846.

Shen, G., Cui, W., Zhang, H., Zhou, F., Huang, W., Liu, Q., Yang, Y., Li, S., Bowman, G.R., Sadler, J.E., *et al.* (2017). Warfarin traps human vitamin K epoxide reductase in an intermediate state during electron transfer. Nat Struct Mol Biol *24*, 69-76.

Solis-Herrera, C., Triplitt, C., Cersosimo, E., and DeFronzo, R.A. (2000). Pathogenesis of Type 2 Diabetes Mellitus. In Endotext, K.R. Feingold, B. Anawalt, A. Boyce, G. Chrousos, W.W. de Herder, K. Dhatariya, K. Dungan, J.M. Hershman, J. Hofland, S. Kalra, *et al.*, eds. (South Dartmouth (MA)).

Srikanth, S., Jew, M., Kim, K.D., Yee, M.K., Abramson, J., and Gwack, Y. (2012). Junctate is a Ca2+-sensing structural component of Orai1 and stromal interaction molecule 1 (STIM1). Proc Natl Acad Sci U S A *109*, 8682-8687.

Srour, B., Fezeu, L.K., Kesse-Guyot, E., Alles, B., Debras, C., Druesne-Pecollo, N., Chazelas, E., Deschasaux, M., Hercberg, S., Galan, P., *et al.* (2020). Ultraprocessed Food Consumption and Risk of Type 2 Diabetes Among Participants of the NutriNet-Sante Prospective Cohort. JAMA Intern Med *180*, 283-291.

Stamateris, R.E., Sharma, R.B., Hollern, D.A., and Alonso, L.C. (2013). Adaptive beta-cell proliferation increases early in high-fat feeding in mice, concurrent with metabolic changes, with induction of islet cyclin D2 expression. American journal of physiology Endocrinology and metabolism *305*, E149-159.

Stenflo, J., Fernlund, P., Egan, W., and Roepstorff, P. (1974). Vitamin K dependent modifications of glutamic acid residues in prothrombin. Proc Natl Acad Sci U S A *71*, 2730-2733.

Thorens, B., Tarussio, D., Maestro, M.A., Rovira, M., Heikkila, E., and Ferrer, J. (2015). Ins1(Cre) knock-in mice for beta cell-specific gene recombination. Diabetologia *58*, 558-565.

Treves, S., Feriotto, G., Moccagatta, L., Gambari, R., and Zorzato, F. (2000). Molecular cloning, expression, functional characterization, chromosomal localization, and gene structure of junctate, a novel integral calcium binding protein of sarco(endo)plasmic reticulum membrane. J Biol Chem *275*, 39555-39568.

bioRxiv preprint doi: https://doi.org/10.1101/2022.05.13.491370; this version posted May 13, 2022. The copyright holder for this preprint (which was not certified by peer review) is the author/funder, who has granted bioRxiv a license to display the preprint in perpetuity. It is made available under aCC-BY-NC 4.0 International license.

Treves, S., Franzini-Armstrong, C., Moccagatta, L., Arnoult, C., Grasso, C., Schrum, A., Ducreux, S., Zhu, M.X., Mikoshiba, K., Girard, T., *et al.* (2004). Junctate is a key element in calcium entry induced by activation of InsP3 receptors and/or calcium store depletion. J Cell Biol *166*, 537-548.

Via, M. (2012). The malnutrition of obesity: micronutrient deficiencies that promote diabetes. ISRN endocrinology *2012*, 103472.

Wang, I.M., Zhang, B., Yang, X., Zhu, J., Stepaniants, S., Zhang, C., Meng, Q., Peters, M., He, Y., Ni, C., *et al.* (2012). Systems analysis of eleven rodent disease models reveals an inflammatome signature and key drivers. Mol Syst Biol *8*, 594.

Yong, J., Parekh, V.S., Reilly, S.M., Nayak, J., Chen, Z., Lebeaupin, C., Jang, I., Zhang, J., Prakash, T.P., Sun, H., *et al.* (2021). Chop/Ddit3 depletion in beta cells alleviates ER stress and corrects hepatic steatosis in mice. Sci Transl Med *13*.

Zhang, I.X., Ren, J., Vadrevu, S., Raghavan, M., and Satin, L.S. (2020). ER stress increases store-operated Ca(2+) entry (SOCE) and augments basal insulin secretion in pancreatic beta cells. J Biol Chem *295*, 5685-5700.

Zwakenberg, S.R., Remmelzwaal, S., Beulens, J.W.J., Booth, S.L., Burgess, S., Dashti, H.S., Imamura, F., Feskens, E.J.M., van der Schouw, Y.T., and Sluijs, I. (2019). Circulating Phylloquinone Concentrations and Risk of Type 2 Diabetes: A Mendelian Randomization Study. Diabetes *68*, 220-225.

bioRxiv preprint doi: https://doi.org/10.1101/2022.05.13.491370; this version posted May 13, 2022. The copyright holder for this preprint (which was not certified by peer review) is the author/funder, who has granted bioRxiv a license to display the preprint in perpetuity. It is made available under aCC-BY-NC 4.0 International license.

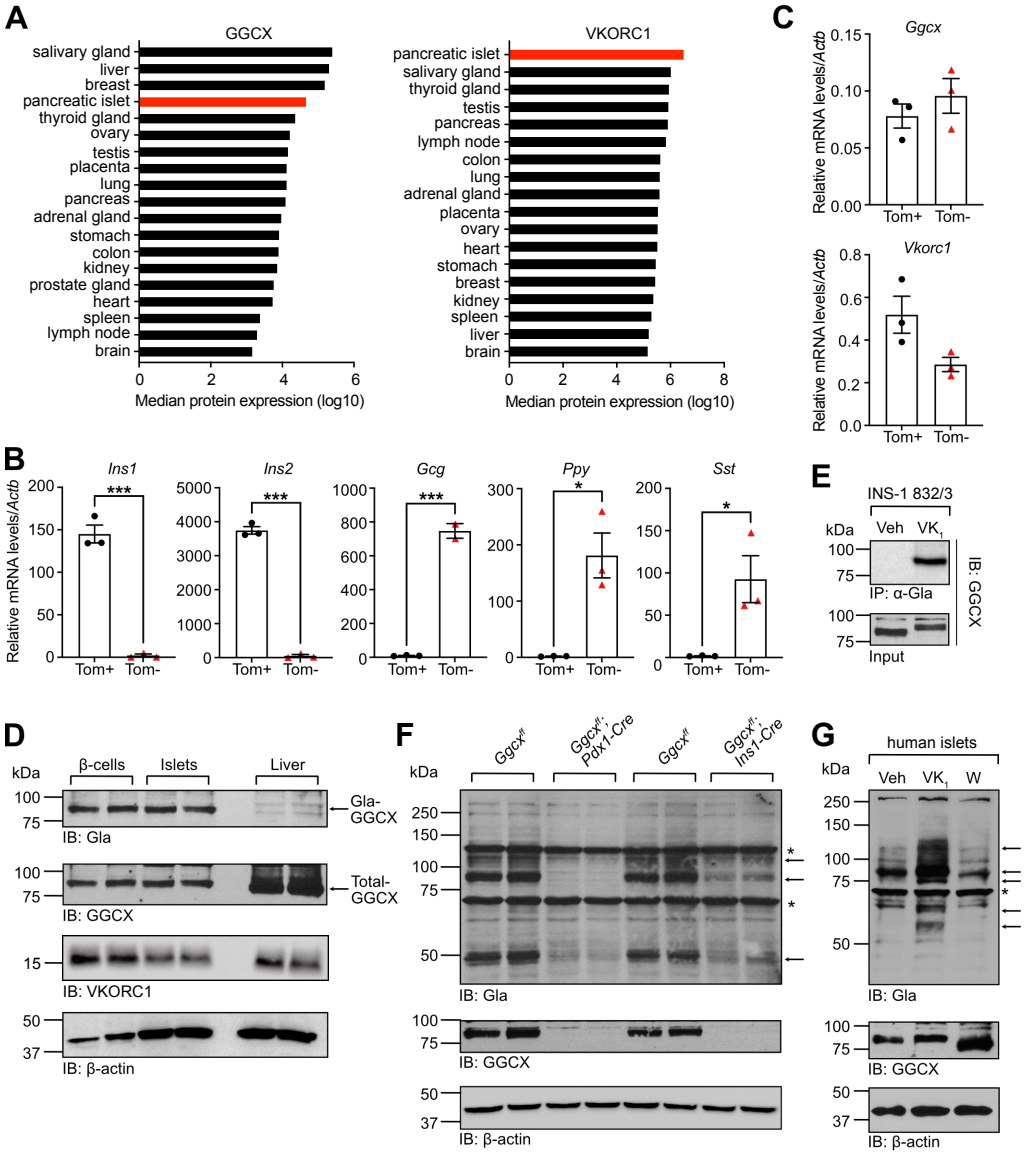

Figure 1

bioRxiv preprint doi: https://doi.org/10.1101/2022.05.13.491370; this version posted May 13, 2022. The copyright holder for this preprint (which was not certified by peer review) is the author/funder, who has granted bioRxiv a license to display the preprint in perpetuity. It is made available under aCC-BY-NC 4.0 International license.

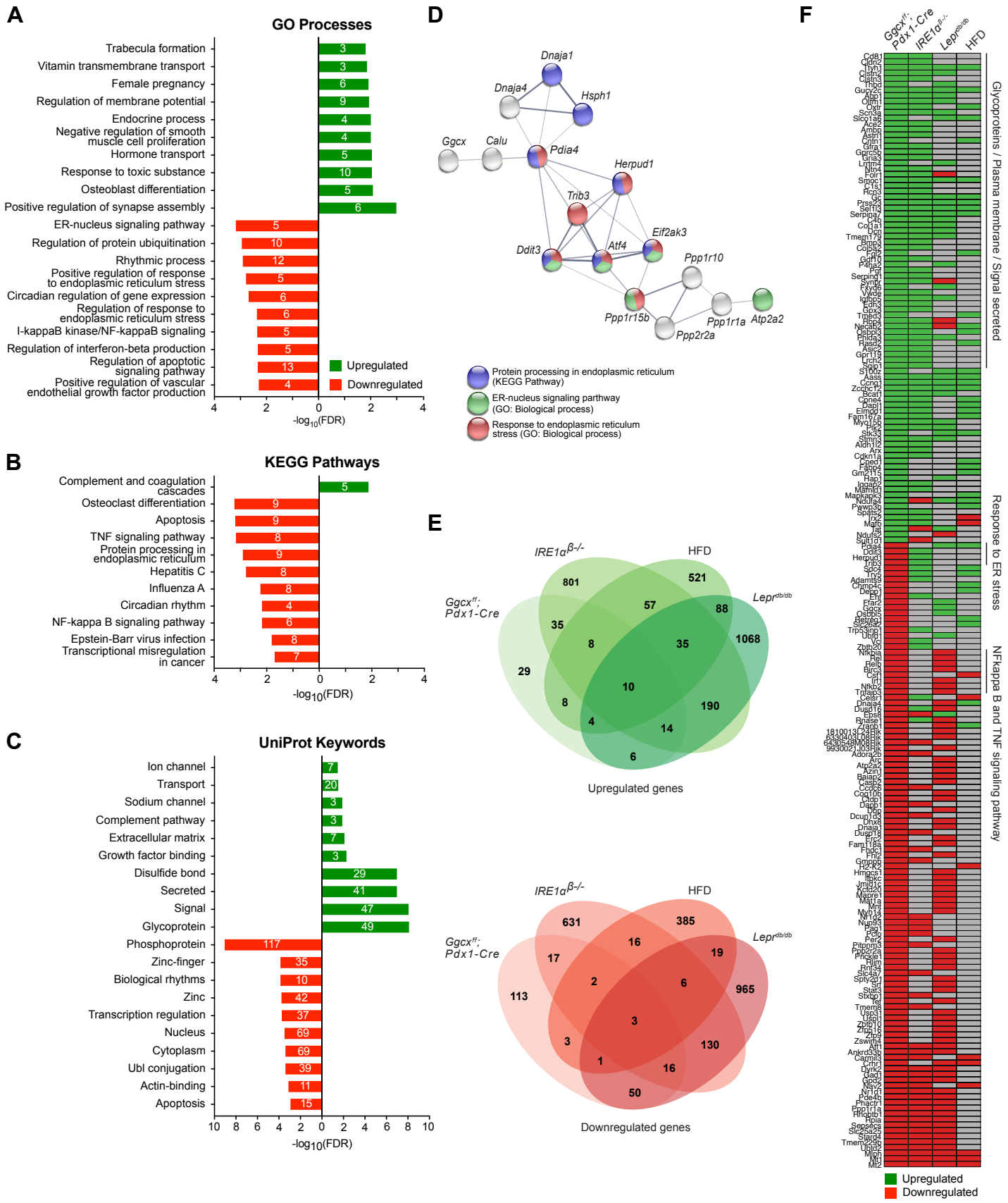

Figure 2

bioRxiv preprint doi: https://doi.org/10.1101/2022.05.13.491370; this version posted May 13, 2022. The copyright holder for this preprint (which was not certified by peer review) is the author/funder, who has granted bioRxiv a license to display the preprint in perpetuity. It is made available under aCC-BY-NC 4.0 International license.

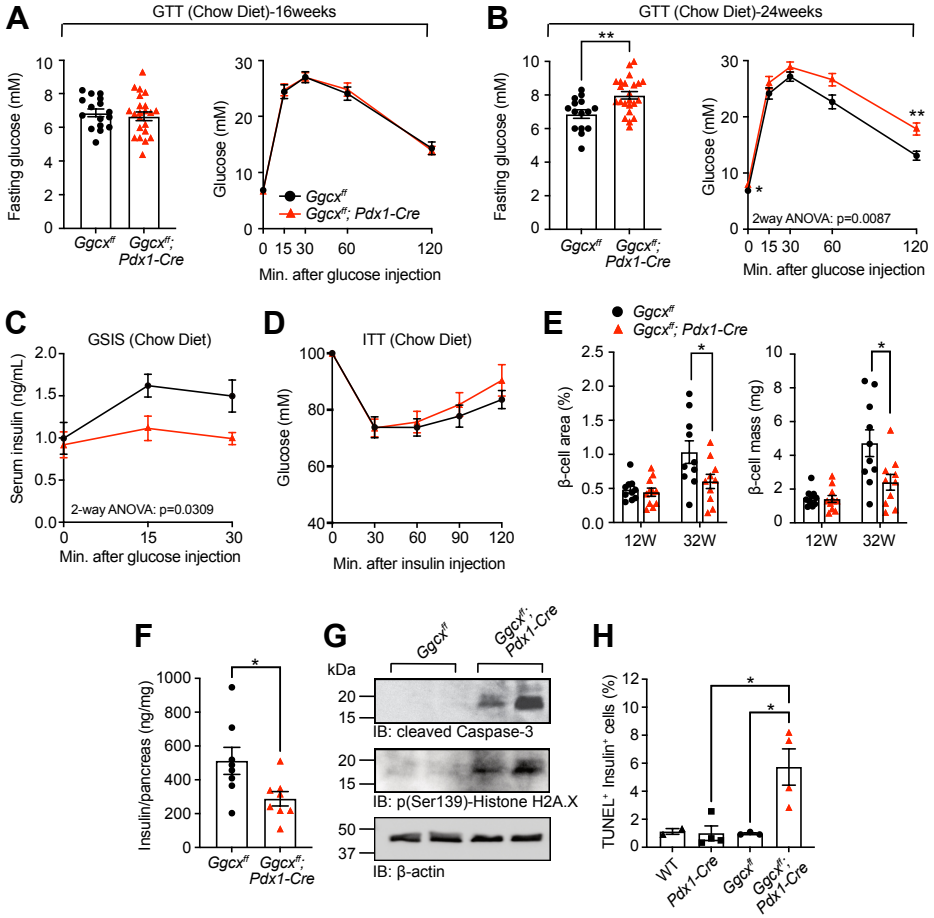

Figure 3

bioRxiv preprint doi: https://doi.org/10.1101/2022.05.13.491370; this version posted May 13, 2022. The copyright holder for this preprint (which was not certified by peer review) is the author/funder, who has granted bioRxiv a license to display the preprint in perpetuity. It is made available under aCC-BY-NC 4.0 International license.

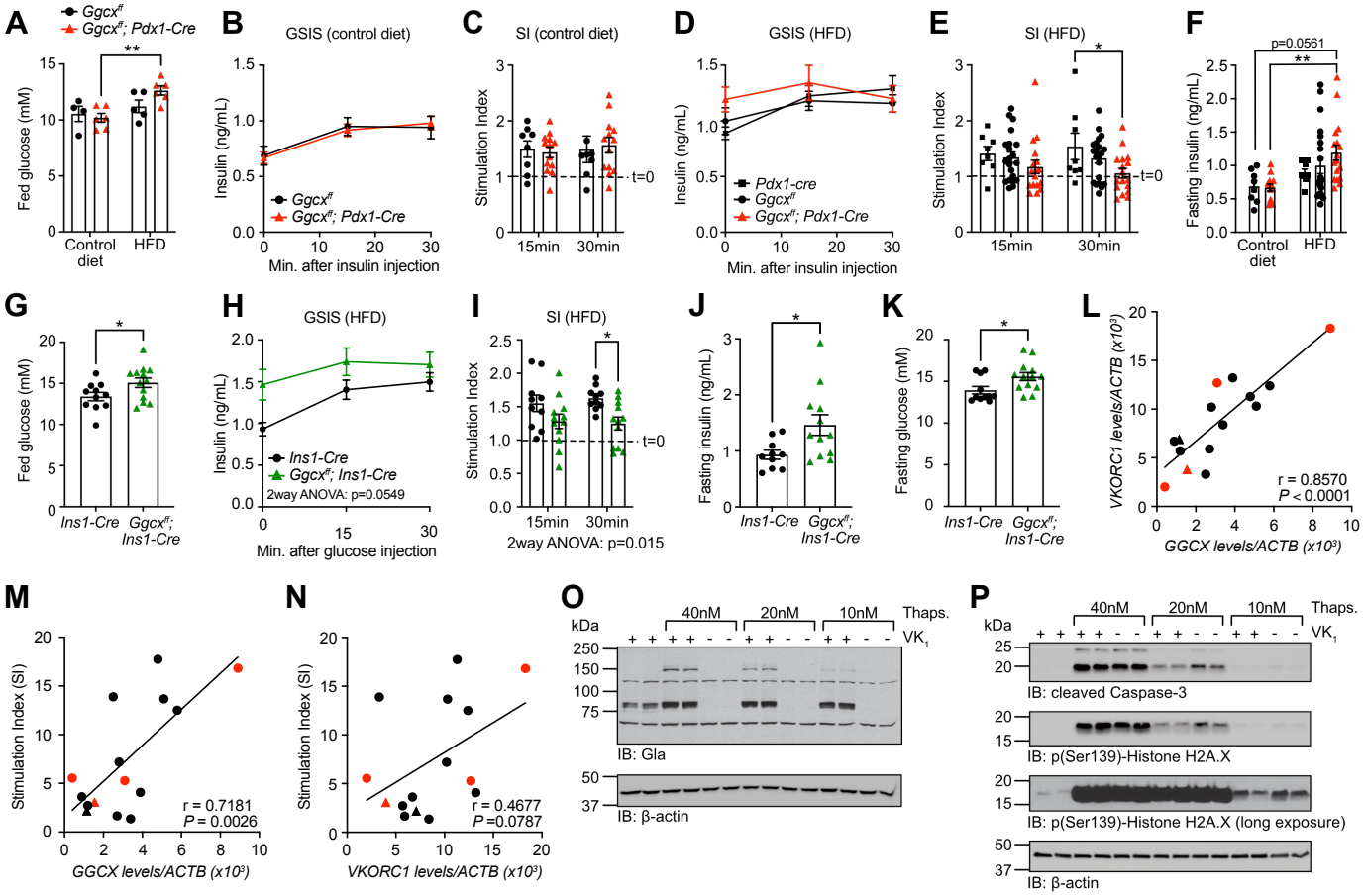

Figure 4

bioRxiv preprint doi: https://doi.org/10.1101/2022.05.13.491370; this version posted May 13, 2022. The copyright holder for this preprint (which was not certified by peer review) is the author/funder, who has granted bioRxiv a license to display the preprint in perpetuity. It is made available under aCC-BY-NC 4.0 International license.

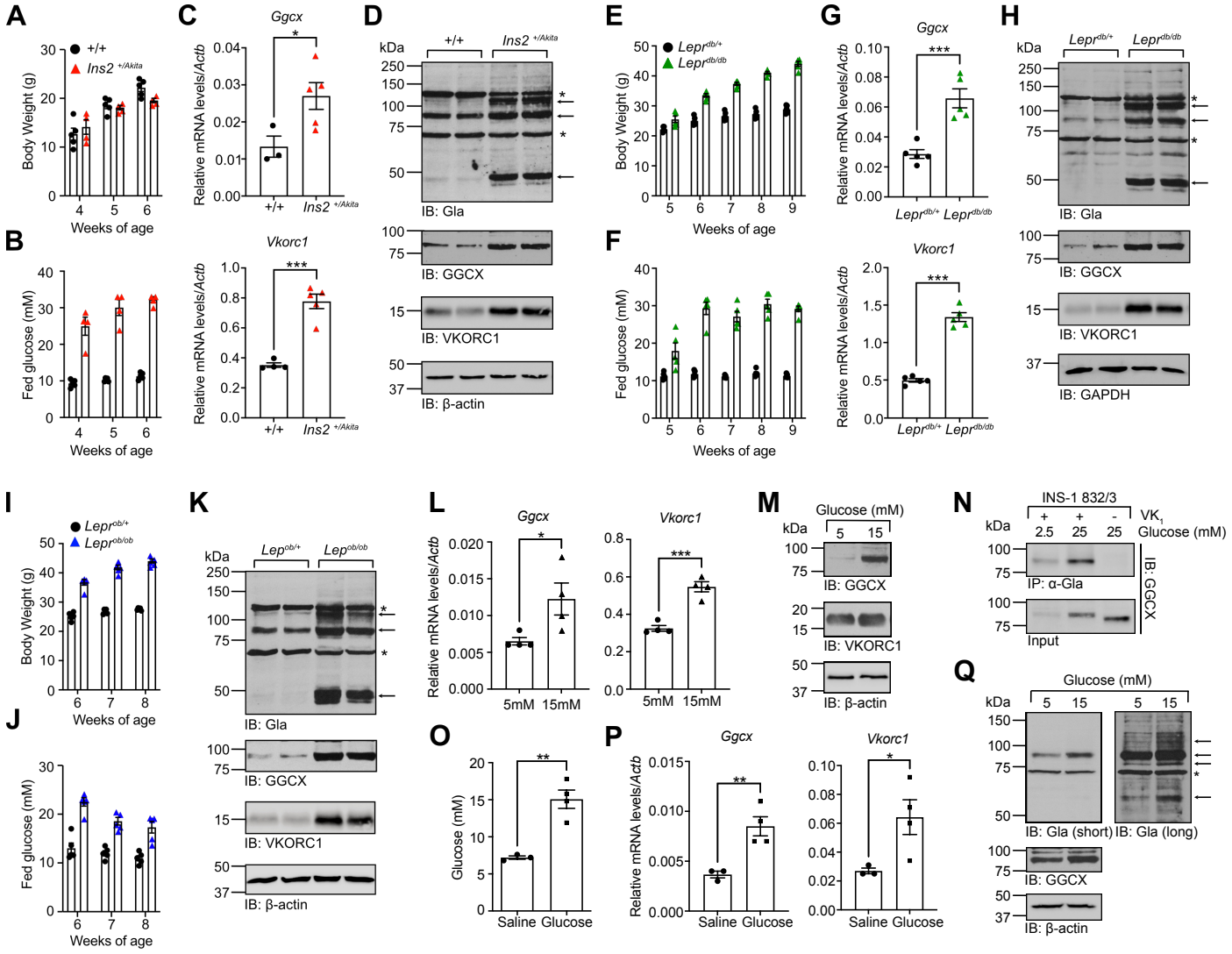

Figure 5

bioRxiv preprint doi: https://doi.org/10.1101/2022.05.13.491370; this version posted May 13, 2022. The copyright holder for this preprint (which was not certified by peer review) is the author/funder, who has granted bioRxiv a license to display the preprint in perpetuity. It is made available under aCC-BY-NC 4.0 International license.

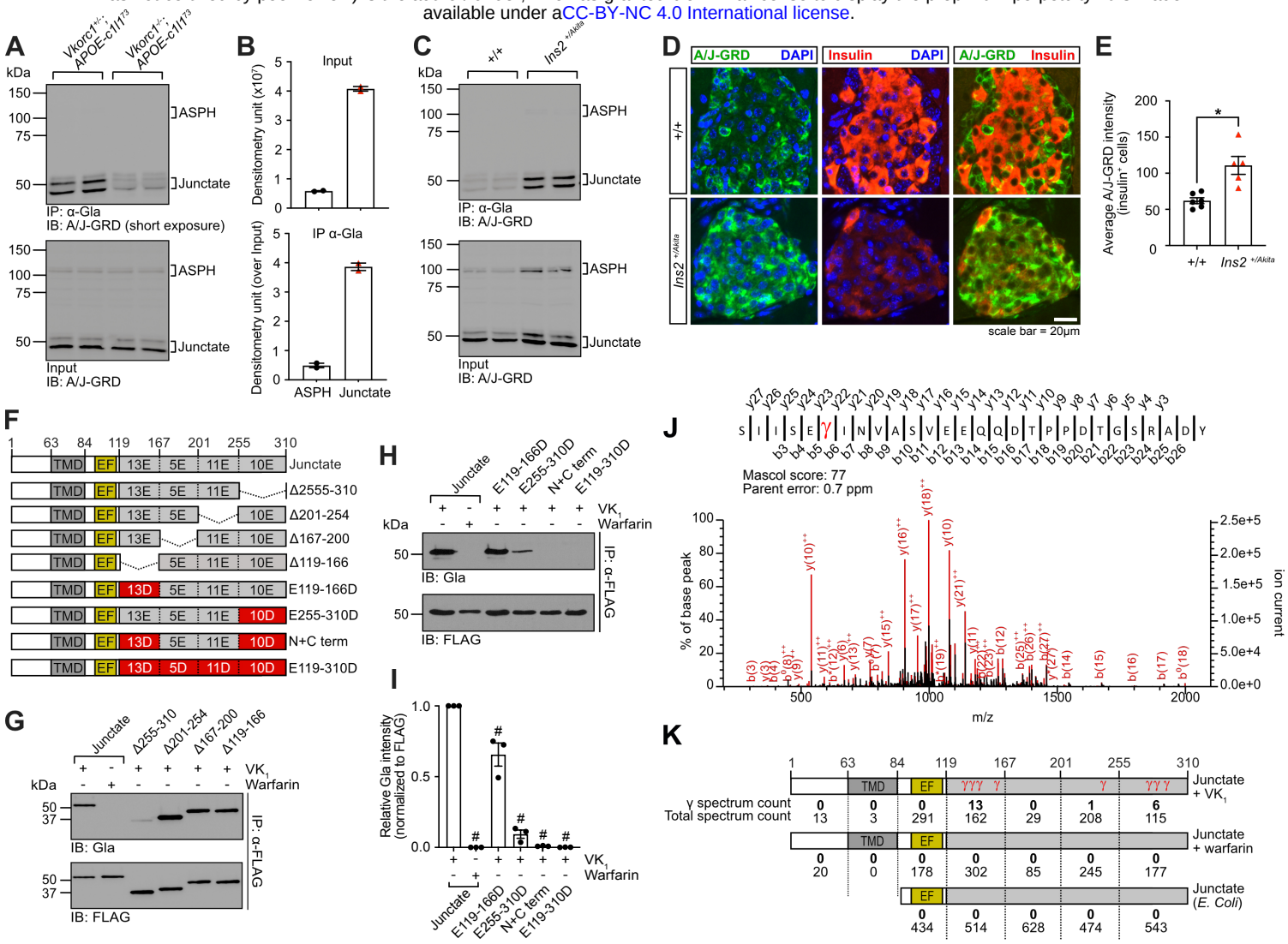

Figure 6

bioRxiv preprint doi: https://doi.org/10.1101/2022.05.13.491370; this version posted May 13, 2022. The copyright holder for this preprint (which was not certified by peer review) is the author/funder, who has granted bioRxiv a license to display the preprint in perpetuity. It is made available under aCC-BY-NC 4.0 International license.

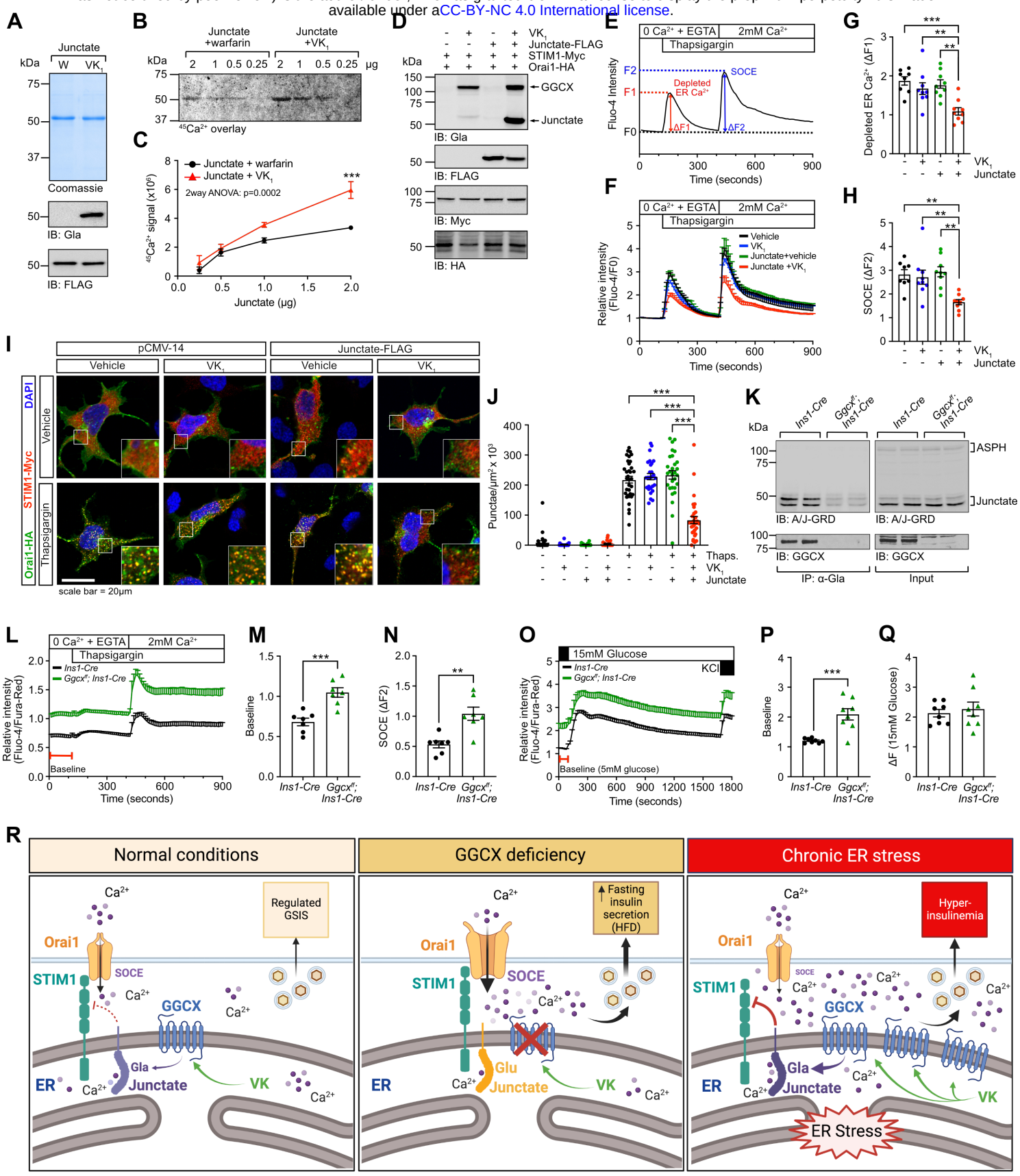

Figure 7